Development of a balloon-borne instrument for CO_2 vertical profile observations in the troposphere

(対流圏 CO_2 高度分布の観測用の気球搭載計測器の開発)

Mai Ouchi

大内麻衣

Nagoya University

2020

和文概要

産業革命以降、人類による化石燃料や天然ガスの膨大な消費により、大気中の二酸化炭素（CO_2）の濃度は急激に増大している。この大気中の CO_2 の濃度の増大が、地球温暖化問題の主要な原因と考えられている。従って、大気中の CO_2 濃度の増大を抑える対策を取るためには、正確にいろいろな場所での CO_2 の濃度を計測することが必要である。しかしながら、現状では CO_2 濃度の計測サイトは充分でなく、とくに高度方向の情報が少ないので、CO_2 の排出や消失過程に関する不確かさが大きい。CO_2 の濃度を地表から上空まで計測する従来の方法としては、飛行機観測が唯一のものであり、経費や観測場所の制限から観測地点数や頻度が極めて限られ長期継続性が困難である。また、GOSAT や OCO-2 などの衛星は、世界各地を定期的に観測しているが、晴天時のそれぞれの地点における地表面から大気上面までの CO_2 濃度の平均値（カラム平均濃度）だけで、高度分布が求められていないので、カラム濃度の増減の要因までは良くわからない。

本研究では、大気中 CO_2 混合比を高度約 10 km まで計測できる気球搭載型 CO_2 計測装置(CO_2 ゾンデ)を開発した。CO_2 ゾンデは、持ち運びができ低電力で CO_2 高度分布の計測を行うことができ、GPS ゾンデを併載しているので気象条件(気温, 湿度, 高度, 場所)を観測することができる。低コストでの観測を実現させるため、非分散型赤外分光法(NDIR)を用いたセンサを独自に開発した。この計測器では、導入した大気の波長 4.0 および 4.3μm でのセル透過光を測定して、CO_2 の光吸収のある 4.3μm での光吸収量を算出することにより CO_2 の濃度を求める。測定の確度を保つため、2 種類の既知濃度の標準ガスをアルミバッグに入れて気球に併載し、40 秒毎に外気と交互に測定することにより、飛揚中に校正を行うシステムを作成した。気球の上昇速度は 3～5 m/s なので、CO_2 濃度測定の高度分解能は 240～400 m 程度になる。計測装置は、NDIR センサの他、制御用の CPU ボード、ガス流路切替バルブ、ピストンポンプなどから構成されている。CO_2 センサからの信号は制御ボードによりデジタル数値化し、GPS ゾンデを通じて地上の受信機に送る。

本研究で開発した CO_2 ゾンデの測定精度を確かめるため、低圧チャンバーを使用した室内実験を行った。その結果、精度は地上(1010 hPa)での精度は 0.6 ppm, 高度 10 km(250 hPa)では 1.2 ppm であった。さらに実際に気球に搭載して測定を行い、ほぼ同時に行われた航空機による CO_2 高度分布の測定結果と比較した。比較に用いた航空機データは、1 つは日本航空(JAL)の定期航空機を利用した大気観測 CONTRAIL プロジェクトで得られた CO_2 データであり、もう 1 つは、温室効果ガス観測技術衛星（GOSAT）の検証のために JAXA および国立環境研究所(NIES)が行ったチャーター航空機による CO_2 の観測データである。2011 年

1 月 31 日と 2 月 3 日につくば市に近い守谷市で放球した 2 つの気球計測の結果と航空機観測の比較から、開発した CO_2 ゾンデの測定精度が、地上から高度 7km までの範囲でバイアスが+0.6 ppm、精度が 1.2 ppm であることがわかった。

さらに、北海道母子里および茨城県守谷市での昼間の気球放球試験を行い、CO_2 の高度分布を得ている。森林地帯の母子里では、CO_2 の高度分布に、昼間の光合成による CO_2 の減少している様子が地表から高度 3km の大気境界層内で明瞭に現れた。首都圏の守谷では地表の交通などの化石燃料燃焼の放出による増大の様子が、地表から高度 2km の大気境界層内で明瞭に現れた。

開発した気球 CO_2 ゾンデは、様々な場所で測定できる、高度分布が測定できる、雲が存在しても測定できる。という特徴があり、時間や場所を選ばずに高い高度分解能で測定ができる。という利点がある。今回開発したコストの低い気球搭載 CO_2 ゾンデで高度分布が各地で観測できるようになり、地球温暖化の最も重要な原因物質である二酸化炭素についても綿密な観測が可能になると、将来の気候変化の予測の精度を飛躍的に高めることが期待される。

Abstract

The atmospheric carbon dioxide (CO_2) concentration has drastically increased since the Industrial Revolution due to the mass consumption of fossil fuels and natural gas by human activities. The increase of atmospheric CO_2 concentration is the most important anthropogenic greenhouse gas contributing to global warming. Therefore, it is important to measure atmospheric CO_2 concentrations correctly to take measures to the increase of CO_2 concentrations. However, owing to the limited number of observation sites and the limitations of their altitudinal range, regional CO_2 sources and sinks have large uncertainties in current estimates. Especially, CO_2 vertical profile measurements are the key to estimate CO_2 sources and sinks in high precision.

We have developed a unique observation instrument for measuring tropospheric carbon dioxide (CO_2) concentration using a small balloon (CO_2 sonde) carrying a non-dispersive infrared (NDIR) analyzer at the wavelengths of 4.0 and 4.3 micrometers. The CO_2 sensor installed in a package with a control board, valves and a piston pump. The instrument is accompanied with a GPS sonde. The NDIR data of CO_2 concentration are transmitted to a ground- based receiver through a GPS sonde with pressure, temperature, humidity and wind data every second. Onboard calibrations using CO_2 standard gas make it possible to measure CO_2 vertical profiles accurately with 240–400 m altitude resolution.

The standard deviations (1σ) of the measured mixing ratios for measurements in a vacuum chamber with temperature 298 K were about 0.6 ppm and 1.2 ppm at 1010 hPa and 250 hPa, respectively. From comparison with the aircraft data, although the difference up to the altitude of 7 km was 0.6±1.2 ppm, this bias and difference lied within the precision of the CO_2 sonde. In field experiments, the CO_2 sonde captured CO_2 increase in urban area and decrease in forest area near the surface. The CO_2 sonde is shown to be

a useful instrument for CO_2 vertical profile observation in the troposphere.

The results of three field experiments using the CO_2 sonde over Moshiri in Japan on 26August 2009 and over Moriya in Japan on 31 January and 3 February, 2011 are presented. These observations showed distinctive profiles of CO_2 at each site. The decrease in CO_2 over Moshiri in the boundary layer was attributed to photosynthesis by trees and grasses around the launching site, whereas the significant enhancement of CO_2 observed near the surface over Moriya was due to anthropogenic emissions.

Contents

Chapter 1

Introduction

1.1. Carbon dioxide (CO_2) in the atmosphere

The earth's atmosphere is commonly described as a series of layers defined by their thermal characteristics. From the lowest region, each layer is referred to as the troposphere, the stratosphere, the mesosphere, and the thermosphere. The troposphere's depth is approximately 10 km in the high latitudes and 18 km in the low latitudes. The temperature in the troposphere decreases with increasing altitude up to a minimum temperature in the troposphere at the region called as the tropopause separating the troposphere from the stratosphere. In contrast, the stratospheric temperature increases with altitude increase because of the ozone layer absorption to the sun radiation until approximately 50 km of the stratopause with the highest temperature in the stratosphere. Above the stratopause, the mesosphere is located up to the altitude of 85 km of the mesopause with the temperature falls as altitude increased again due to absorptions to ultraviolet by N_2 and O_2 emitted strongly from the sun. In the thermosphere, located above the mesopause, the temperature increase with altitude.

Although, the atmospheric thickness is approximately 1000 km, the total mass of 99.9% is in the troposphere and the stratosphere. Especially for the troposphere, it has approximately 85% of the total mass averaged by the earth. The earth's atmosphere is almost composed of N_2, O_2, and Ar for ratio of 78%, 21%, and 0.9%, respectively. Rest of the 0.1% is mainly constitute of CO_2, Ne, O_3, and N_2O, called as trace gases. In spite of low concentration of the trace gases, they play important roles of the environmental issues such as global warming, ozone depletion, and smog.

Atmospheric CO_2 is an important greenhouse gas, second only to water vapor. In order

to understand the meaning of greenhouse gases and greenhouse effect, it is needed to know about earth's temperature system. The sun provides energy to the earth as radiation, then, it is converted to thermal energy at the surface. The surface heated by the solar radiation emits the infrared radiation to be absorbed by the trace gases such as CO_2, O_3, N_2O, CH_4. The greenhouse gases have each absorption band in corresponding to the thermal energy from the earth, and increases such gases in the atmosphere results trapping more of the thermal energy. CO_2 has strong absorption at 2.7, 4.3, 15 μm and weak absorption 1.4, 1.6, 5, 10 μm. Fifteen μm is a peak of the thermal radiation energy from the earth, and CO_2 amount in the atmosphere influences strongly to the earth's energy balance.

CO_2 mixing ratio is described as CO_2 mole fractions per dry air mole fractions or CO_2 volume by dry air volume (IPCC, 2013). Mixing ratio can be written in mol/mol or volume/volume as the same meaning in the case of the ideal gas, defined as a hypothetical gas under the conditions of neither molecular attraction nor volume of molecules. In the ideal gas, the volume occupied with gas is proportional to the number of molecules. In the case of actual gas on the earth, it can be applied the ideal gas law. CO_2 mixing ratio expressed by mol/mol is equal to volume/volume. The following abbreviation is used for CO_2 mixing ratio: ppm (perts per million).

Atmospheric carbon dioxide (CO_2) is the most important anthropogenic greenhouse gas contributing to global warming. Atmospheric CO_2 has been increasing because of human activities, such as fossil fuel combustion, cement production, and deforestation. Figure 1 shows the temporal behaviors of atmospheric concentrations of carbon dioxide (CO_2) from Mauna Loa and South Pole since 1958 (IPCC, 2013). The global average concentration of atmospheric CO_2 has increased from 280 ppm before the Industrial

Revolution to 400.0 ppm in 2015 (World Meteorological Organization, WMO 2016). The growth rate of atmospheric CO_2 has been measured at 2.3 ppm yr^{-1} from 2014 to 2015 (WMO 2016).

As shown in the Figure 2 taken from ESA web site, the flying carpet, it is found from atmospheric measurements that carbon sources and sinks at the surface have variations depending on place and time. Atmospheric CO_2 indicates seasonal changes; low value of the CO_2 mixing ratio in summer because of high photosynthesis value of the CO_2 mixing ratio and in winter by plants respiration and fossil fuel combustion for heating appliance. The northern hemisphere had an amplitude larger than that of the southern hemisphere due to larger land area and heavy population compared to those of the southern hemisphere.

1.2. Observations of CO_2 concentration in the atmosphere

Atmospheric CO_2 has been measured by ground-based stations and ships using flask sampling or continuous measurement instruments such as non-dispersive infrared absorption (NDIR) (Tanaka et al. 1983) and cavity ring-down spectroscopy (CRDS) (Winderlitch et al. 2010) systems. Figure 3 shows the principle of the NDIR instrument. The light intensities at the two wavelengths of 4.0 μm (out of the CO_2 absorption band) and 4.3 μm (in CO_2 absorption band) through the air sample tube are measured and the concentration of CO_2 is determined. For the selection of the wavelengths at the 4.0 and 4.3 μm, band-pass filters are used which have relatively broad band characteristics. As shown in Figure 4, for the continuous CO_2 NDIR measurements not only absorption cell system but also standard gases and valve system are required. Recently the CRDS instruments have been used in monitoring sites. Figure 5 shows the principle of the CRDS

measurements. A pulsed narrow-band infrared diode laser is used as a light source. The decay time of the laser light intensities are measured through a cavity containing the air sample with mirrors (high reflectance, R > 99.99%). A network of ground-based Fourier transform spectrometers (FTS) that records direct solar spectra in the near-infrared spectral region (Total Carbon Column Observing Network, TCCON) has observed the column-averaged mole fraction of CO_2 in dry air; total column XCO_2 (Wunch et al. 2011). These observations have provided extensive information respecting distribution and temporal variation of CO_2 in the atmosphere (Pales and Keeling, 1965; Conway et al. 1988, 1994; Komhyr et al. 1989; Tans et al. 1989). Moreover, atmospheric CO_2 measurements data are useful for estimates of CO_2 fluxes on the surface through inverse modeling (Gurney et al. 2004; Baker et al. 2006). However, owing to the limited number of observation sites and the limitations of their altitudinal range, regional CO_2 sources and sinks have large uncertainties in current estimates (Gurney et al. 2002). More atmospheric CO_2 measurements are needed to reduce the uncertainties in CO_2 fluxes estimation using inverse modeling.

To solve the insufficient observational CO_2 data issue, several observations of greenhouse gases using satellite remote sensing have been used to investigate the CO_2 distribution on a global scale (Chédin et al. 2002; Crevoisier et al. 2004; Dils et al. 2006). The Greenhouse gases Observing SATellite (GOSAT) measures a Short Wavelength IR (SWIR) total column atmospheric absorption spectrum of CO_2, from which total column XCO_2 can be estimated, which has been in operation since early 2009 (Yokota et al. 2009; Yoshida et al. 2011; Morino et al. 2011). The Orbiting Carbon Observatory-2 (OCO-2) satellite also measures total column XCO_2 since 2014 (Eldering et al. 2017).

Because SWIR satellite measurement can only measure total column XCO_2, we need

other techniques for vertical measurement of CO_2. For instance, tall towers measure CO_2 vertical profiles near the ground (Bakwin et al. 1992, Inoue and Matsueda, 2001; Andrews et al. 2014). CO_2 vertical profiles up to 10 km around airports have been observed by commercial airlines such as the Comprehensive Observation Network for TRace gases by Airliner (CONTRAIL program) (Machida et al. 2008; Matsueda et al. 2008). Chartered aircrafts measurements, for instance, the High-performance Instrumented Airborne Platform for Environmental Research (HIAPER) Pole-to-Pole Observations (HIPPO) program up to 14 km in the altitude spanning the Pacific from 85° N to 67° S (Wofsy et al. 2011), NIES/JAXA (National Institute of Environmental Studies and Japan Aerospace eXploration Agency) program in the altitude from 2 to 7 km (Tanaka et al. 2012), and NOAA/ESRL Global Greenhouse Gas Reference Network Aircraft Program (Sweeney et al. 2015) were performed. Although these aircraft measurements enable the atmospheric CO_2 concentration data to be increased globally, some sparse observation coverage remained such as tropics.

Atmospheric CO_2 observations using balloons, which are available to choose locations unless prohibited or restricted areas for flight, are helpful to solve the sparseness of CO_2 vertical data. Balloon observations for stratospheric CO_2 were conducted by some groups. For instance, stratospheric air sampling has been conducted using cryogenic sampler onboard balloons once a year from 1985 to 1995 over the northern part of Japan (Nakazawa et al. 1995). A balloon-borne near-infrared tunable diode laser spectrometers have been developed to provide in situ data for CO_2 in the stratospheric atmosphere (Durry et al. 2004; Joly et al. 2007, Ghysels et al. 2012). Furthermore, two in-situ CO_2 analyzers adopted by NDIR technique using a modified commercial detector for stratospheric measurements have been developed for deployment on the NASA ER-2

aircraft and on a balloon (Daube et al. 2002).

1.3. CO_2 vertical profiles in the troposphere

The CO_2 vertical profile in the troposphere is considered to have the structure such a schematic diagram of Figure 6. The CO_2 until 2- 3 km in the altitude (called as the boundary layer) is greatly influenced by local emissions and uptakes. CO_2 sources and sinks occur at the surface by photosynthesis, respiration, and human activities. Thus, CO_2 mixing ratio in the boundary layer can be changed largely reflected by short-distance effect of CO_2 emission and intake at the surface. The CO_2 mixing ratio in the boundary layer is introduced into free troposphere within a few days as pictured in Figure 6 in the relation with temporal and spatial scales of CO_2. The CO_2 mixing ratio in the free troposphere as defined above the boundary layer is impacted by the middle/long-range transport air parcel (Shirai et al., 2012). CO_2 mixing ratio in the free troposphere is not as variable as CO_2 mixing ratio in the boundary layer. Stratospheric CO_2 is thought to be almost uniform and its mixing ratio is reflected CO_2 mixing ratio in the boundary layer 2 or 3 years behind (Nakazawa et al. 2002). Therefore, CO_2 vertical profile is not always uniform. It is needed for CO_2 vertical profile measurement with high precision.

1.4. The aim of this thesis

To restrain the climate change such as global warming, the emission of CO_2 due to human activities should be reduced. It is required to explore the regional and global CO_2 fluxes correctly for the implement of efficient political activities to reduce the emissions of CO_2. We need to make clear the contribution of each category of CO_2 emission such

as power plants, motor vehicles, forest fire, peat fire, improvements of land usage, and tree planting etc. Also, it is important to estimate CO_2 fluxes precisely from each country. However , direct measurements of CO_2 emission fluxes are very difficult. On the other hand, CO_2 mixing ratio measurements in the atmosphere are relatively easy for everywhere in the world. The CO_2 mixing ratio is determined by CO_2 releasing from emission sources, CO_2 sink into forests and ocean, and transportation with diffusion by wind. We can measure the atmospheric CO_2 at various locations. In addition, numerical model calculations can also estimate the CO_2 mixing ratios in the atmosphere using the assumption of the CO_2 emission from the consumption of fossil fuels and uptake from the forests and ocean. However, the differences between the models and actual measurements in the CO_2 mixing ratio values often occur. The main cause of the differences is the error in the assumption of the CO_2 sources and sinks in the model calculations. The inverse model calculations based on the actual CO_2 mixing ratio values in the atmosphere by measurements can be good solutions for the calculation of CO_2 emission sources and sinks more correctly. Additionally, the CO_2 vertical mixing ratio measurements are necessary to reduce the estimation errors in the inverse modeling. For example, by adding the CO_2 vertical profile data to the surface data the model calculations are greatly improved about 64% in the tropics (Niwa et al. 2012).

For now, lack of the CO_2 vertical measurement data is a big problem for precise estimations by inverse modeling about the locations and quantities of CO_2 sources and sinks. Therefore, it is needed to measure CO_2 vertical profiles in the troposphere by a new method. We developed a balloon-borne measurement instrument for tropospheric CO_2 vertical profiles.

Chapter 2

Description of the CO_2 balloon-borne system

2.1. Instrumentation

The CO_2 sonde is a lightweight balloon-borne instrument combined with a GPS radiosonde (Meisei Electric co., Ltd., RS-06G). The balloon carries the instrument packages in the altitude with measuring CO_2 and meteorological data (GPS position and time, temperature, pressure, and humidity). The CO_2 sonde transmits those data to a ground receiver (Meisei Electric co., Ltd., RD-08AC) at 1 s intervals, thus it is unnecessary to recover the CO_2 sonde after the balloon burst. Figure 7 shows an overall view of the CO_2 sonde developed in this study. It consists of a CO_2 measurement package, a calibration gas package, a GPS radiosonde, a balloon, and a parachute. The total weight of the CO_2 sonde was 1700 g, including the GPS radiosonde (150 g), CO_2 measurement package (1000 g), and calibration gas package (550 g). The size of the CO_2 measurement package was width (W) 280 mm × height (H) 150 mm × depth (D) 280 mm. The size of the calibration gas package was W 400 mm × H 420 mm × D 490 mm.

2.2. CO_2 sensor and observation method

A schematic diagram of the CO_2 measurement instrument is shown in Figure 8. The CO_2 sonde has three inlets installed for ambient air and two calibration gases with mesh filters (EMD Millipore, Millex-HA, 0.45 μm pore size) to remove atmospheric particles. Three solenoid valves (Koganei, G010LE1-21) were used to switch the gas flow to the CO_2 sensor. A constant-volume piston pump of flow rate 300 cm^3 min^{-1} (Meisei Electric co., Ltd.), which was originally used for ozone sonde instruments, directed the gas flows from the inlets through the solenoid valves into a dehumidifier, a flow meter, and a CO_2

sensor. The absolute STP (standard temperature and pressure) flow rate decreased with the pressure decrease. Since the exit port of the CO_2 sensor was open to the ambient air, the pressure of dehumidified outside air and calibration gases in the absorption cell were equal to the ambient pressure during the flight. Next to the pump, the gases were introduced to a glass tube filled with magnesium perchlorate grains (dehumidifier) installed upstream of the CO_2 sensor to remove water vapor. Fabric filters were installed on both ends of the dehumidifier, and a mesh filter was installed downstream of the dehumidifier to prevent the CO_2 sensor from the incursion of magnesium perchlorate grains.

The CO_2 sensor was based on the NDIR technique. The infrared absorption cell consisted of a gold-coated glass tube, a light source, and a photodetector. The light source (Helioworks, EP3963) consisted of a tungsten filament whose spectrum had a peak intensity wavelength of approximately 4 μm. The light from the source passed through a gold-coated glass tube with high reflectance at IR region, length 120 mm, and inside diameter 9.0 mm. The photodetector (Perkin-Elmer TPS2734) had two thermopile elements, one of which was equipped with a band-pass filter at a wavelength of 4.3 μm for the measurement of the CO_2 absorption signal and the other was equipped with a band-pass filter at a wavelength of 4.0 μm for the measurement of the background signal. The signals from the sensors were amplified by an operational amplifier and converted to 16 bit digital values by an A/D convertor. The signal intensities of the detectors at 4.0 and 4.3 μm without CO_2 gas were set to approximately equal levels by adjusting the amplification factors in the laboratory. The electric power for the CO_2 sensor, pump, and valves was supplied through a control board by three 9-V lithium batteries, which can last for more than 3 h during the flight. The control board connected with the components

regulates the measuring procedures such as switching the solenoid valves and sending the data to the GPS radiosonde at 1 Hz.

2.3. Calibration gas package

The changes in the temperature and pressure of the ambient air during the ascent of balloons from the ground to 10 km altitude are typically very large and ranged from ~300 K to ~220 K and from ~1000 hPa to ~250 hPa, respectively. Under these hard conditions, the CO_2 sensor signal is typically unstable during the flight and the calibration of the CO_2 sensor only on the ground before launch is generally insufficient to obtain precise values of the CO_2 concentration within several ppm. To solve this problem, our instrument incorporated an in-flight calibration system for the CO_2 sonde. A calibration gas package was attached to the CO_2 sonde for the in-flight calibration, as shown in Figure 7. The calibration gas package consisted of two aluminum coated polytetrafluoroethylene (PTFE) bags (maximum volume: 20 L) containing reference gases with low (~370 ppm) and high (~400 ppm) CO_2 concentrations. In each bag, ~8 L (STP) of the reference gas was introduced from standard CO_2 gas cylinders before launch. Since the gas bags were soft, their inner pressures were kept to be equal to the ambient air pressures during the balloon flight. The gas volumes in the bags increased with the altitude during ascent of the balloon due to decrease of the ambient pressure, while the reference gases were consumed by the calibration procedures. The optimum gas amounts in the bags were determined by both the ascending speed of the balloon and the consumption rate to avoid the bursting of the bags and exhaustion of the gases. The CO_2 concentrations of the reference gases in the bags were checked by the NDIR instrument (LICOR, LI-840) before launch. After the check, approximately 6 L of the reference gas was left in each

bag for the subsequent in-flight calibration. The change in the CO_2 mixing ratio in the bags was determined to be less than 1 ppm over a 3 days period, and thus was considered to be negligible over the time scale of the balloon observations. All measurements were reported as dry-air mole fractions relative to internally consistent standard scales maintained at Tohoku University (Tanaka et al. 1987; Nakazawa et al. 1992).

The performances of the CO_2 sonde instruments were checked before the balloon launchings. For about 60 min. before the launchings, the values of $[I(4.0)-I(4.3)]/P$ were measured with the valve cycles (each step 40 s, total 160 s) for two standard gas packages (~370 ppm and ~400 ppm) for calibration and one intermediate concentration gas package (~385 ppm) as a simulated ambient gas sample.

2.4. Data analysis method

Figure 9 shows an example of the raw data obtained from the CO_2 sonde experiment. The plots in Figure 9 indicate the values of $[I(4.0)-I(4.3)]/P$ against altitude, where $I(4.0)$ and $I(4.3)$ are the signal intensities at the 4.0 μm wavelength for background measurements and the 4.3 μm wavelength for CO_2 absorption measurements, respectively, as obtained by the NDIR CO_2 sensor on the balloon, and P is the ambient atmospheric pressure obtained by the GPS sonde data and pressure measurements on the ground. The measurement cycle during the flights consisted of the following steps: 1) low concentration standard gas, 2) ambient air, 3) high concentration standard gas, and 4) ambient air. The measurement time for each step was 40 s. At switching timings of the valve cycles the signal became stable within 10 s and the averages of residual 30-s period signals were used for the calculation of the CO_2 mixing ratios. Since the ascending speed of the CO_2 sonde balloon was typically 3–5 m s^{-1}, the original height resolution of the

measurements for the vertical profiles of CO_2 corresponded to approximately 240–400 m.

During the balloon-borne flights the temperatures inside the CO_2 sonde package were measured with thermistors. The temperature inside the CO_2 sonde package gradually fell down about 5 K, from 298 K on the ground to 293 K at the altitude of 10 km during the flights. Within one cycle time (160 s) for the standard gases and ambient air measurements, the temperature change is less than 0.4 K. The temperatures of the sample gas in the tube just before the inlet of the CO_2 NDIR cell were also measured using a thin wire thermistor which is usually used for ambient temperature measurement in a GPS sonde with a quick response time (shorter than 2 s). The gas temperature change was negligible at the valve change timings between the standard gas and ambient air (< 0.1 K). This result indicated that the gas temperatures were almost constant after passing through the valves, pump, dehumidifier cell, and piping for the standard gases and ambient air.

For the calculation of the ambient air CO_2 mixing ratios, a linear interpolation method was used with the values of $[I(4.0)-I(4.3)]/P$ for the ambient air and two standard gases. The usage of the values of $[I(4.0)-I(4.3)]/P$ is related to the Beer–Lambert Law. The Beer–Lambert Law is expressed by defining the light intensity in the absence of CO_2 in the cell as I_0 and the light intensity in the presence of CO_2 in the cell as I, as following Eq. (1):

$$\frac{I}{I_0} = \exp(-\varepsilon C L) \qquad (1),$$

where C is the CO_2 concentration in molecules cm^{-3}, L is optical path length in cm, and ε is the absorption cross-section in cm^2 $molecule^{-1}$. Using the relation of $C = XP(k_B T)^{-1}$, where X is the CO_2 mixing ratio and P is the pressure of

dehumidified ambient air, and the approximation of $\exp(-\varepsilon C L) = 1 - \varepsilon C L$, under the condition of $\varepsilon C L << 1$, Eq. (1) is written as follows:

$$\frac{(I_0 - I)}{P} = X \frac{I_0 \varepsilon L}{k_B T_C} \qquad (2),$$

where T_c is the sample air temperature in the sensor cell and k_B is the Boltzmann constant. The values of $[I(4.0) - I(4.3)]$/P were used instead of $(I_0 - I)$/P to obtain the CO_2 mixing ratio values in the measurements. As shown in Figure 9, the difference of $[I(4.0) - I(4.3)]$/P values between the low and high concentration standard gases were almost constant during the flights. Since there were in-phase fluctuations in the $I(4.0)$ and $I(4.3)$ signals during the flights, the subtraction of $[I(4.0) - I(4.3)]$ could improve the signal-to-noise ratios by canceling in-phase fluctuations with each other.

Since the ambient air and two standard gases were sequentially measured with the NDIR cell (40-s each step), the signal levels of $[I(4.0) - I(4.3)]/P$ values for the standard gases at the timing of the ambient air measurements were estimated using a cubic spline interpolation method for the 40-s average values for the determination of the ambient air CO_2 mixing ratios, as shown in Figure 9. The observed variability in the $[I(4.0) - I(4.3)]/P$ values for the standard gases were probably attributed to the vibration and/or inclination of the CO_2 sonde package caused by wind during the flights, which resulted in errors in the calculation of the CO_2 mixing ratios. In principle, the absorption intensities $(I_0 - I)$ in the NDIR measurements are proportional to the absolute CO_2 concentrations in the sample air in the absorption cell. Therefore, at higher altitudes where the pressures were lower, the values of $[I(4.0) - I(4.3)]$ were small and the signal-to-noise ratios of $[I(4.0) - I(4.3)]/P$ decreased. The upper limit of the altitude for the measurements of CO_2 mixing using the CO_2 sonde was approximately 10

km from the ground due to the low signal-to-noise ratios of $\left[I(4.0)-I(4.3)\right]/P$.

Chapter 3

Performance evaluation of the developed CO_2 sonde

3.1. Laboratory tests

Figure 10 shows the result of an experiment using a vacuum chamber in the laboratory we have simulated the flight pressure conditions and the performances of the CO_2 sonde instruments, where the temperature inside the chamber was not controlled and was about 298 K. The pressure of the chamber was gradually decreased using a mechanical pump from 1010 hPa (ground surface pressure) to 250 hPa (about 10 km altitude pressure) for 60 minutes. The values of $[I(4.0)-I(4.3)]/P$ were measured for the two standard gas packages and in the intermediate concentration gas package with the valve cycles (each step 40 s, total 160 s). The results indicated the fluctuations of the measured mixing ratios were almost proportional to 1 / P. The standard deviation (one sigma) of the CO_2 mixing ratios were 0.6 ppm at 1010 hPa and 1.2 ppm at 250 hPa for the 2 valve cycles.

When the CO_2 sonde instrument was inclined and vibrated in the laboratory, the fluctuations of the signals were observed. The quantitative correlation between the signal fluctuation intensities and acceleration speed values measured by an acceleration sensor was investigated, but no distinct correlation was observed. However, the in-flight calibration system solved this problem by taking the signal difference of $[I(4.0)-I(4.3)]$ and also by measuring alternately the two standard gases every 40 s as reference points.

Since the linear interpolation method with the $[I(4.0)-I(4.3)]/P$ values were used for the determination of the ambient air CO_2 mixing ratios in the balloon-born experiments, the deviations from the linear interpolation process was also investigated. The measurements of various mixing ratio gas samples in the laboratory indicated that the error of the linear interpolation with the two standard gas packages (~370 ppm and

~400 ppm) was less than 0.2 ppm in the range between 360 and 410 ppm.

The temperature characteristics of the CO_2 sensor were also investigated by changing the sensor cell block temperature from 273 to 323 K at the pressure of ~1010 hPa in the laboratory. The laboratory experiment on the temperature dependence suggested that the measurement error is less than 0.2 ppm due to the temperature change during one valve cycle in the balloon-borne experiments.

We conducted an experiment for the effects of water vapor when the CO_2 sonde measure the CO_2 with water vapor. Figure 11 shows the result of the CO_2 sensor experiment for influence of water vapor. The detail of the experiment is as below. The three kind of gases were used for this experiment: 377ppm, 414ppm, 414ppm with water vapor. Three inlets have each gas and directly pumped into the CO2 sensor without dehumidifier. Three gases are introduced into the aluminum coated bags from gas cylinders. 414ppm gas with water vapor was made by through a bottle filled with water by 30 ml. The other two gases were introduced from the gas cylinders to the aluminum coated bags directly. As a result, We found that measuring the gas with water vapor leads to the strange signals like saw waves in both 4.0μm and 4.3μm and unable to measure the CO_2 correctly. When the gas with water vapor flows into the CO_2 sensor, the saw waves appears in the signals. At the CO_2 sonde observations in upper atmosphere, we confirmed the saw waves signals were not detected. Thus, we conclude that there are no effects on the CO_2 sensors from water vapor and clouds.

3. 2. Field observations and comparison with aircraft measurements

Two kinds of aircraft measurement data, the NIES/JAXA chartered aircraft and the CONTRAIL, were used for comparison with the CO_2 sonde measurement data. The

NIES/JAXA chartered aircraft measurements were conducted on the same days as the CO_2 sonde observations (31 January 2011 and 3 February 2011). The chartered aircraft observations were performed as a part of the campaign for validating the GOSAT and calibrating TCCON FTS data at Tsukuba (36.05°N, 140.12°E) (Tanaka et al., 2012). The chartered aircraft data were obtained using an on-board NDIR instrument that had an uncertainty of 0.2 ppm. On both 31 January and 3 February, the chartered aircraft measured the CO_2 mixing ratios during descent spirals over Tsukuba and Kumagaya (Figure 12). Because the air traffic is strictly regulated near the two international airports, Haneda and Narita, aircraft observations at altitudes above 2 km over Tsukuba were prohibited. Therefore, the descent spiral observation was conducted over Kumagaya at altitudes of 7–2 km and over Tsukuba at altitudes of 2–0.5 km. Tsukuba is located approximately 20 km northeast of Moriya and includes forests, agricultural land, and urban areas. Kumagaya is located approximately 70 km northwest of Moriya.

Seven profiles of the CONTRAIL measurement, which were obtained during the ascent and descent of aircrafts over Narita airport and have passage time near to the CO_2 sonde observations, were available within two days after or before the dates of the CO_2 sonde measurements (Table 1). The CO_2 sonde observations were conducted on 31 January and 3 February 2011 at Moriya. One set of CONTRAIL data obtained on the flight from Hong Kong to Narita (data set name: 11_060d) was available for 31 January, but no CONTRAIL data were available for 3 February. Therefore, the CONTRAIL data obtained on the flight from Hong Kong to Narita on 2 February (data set name: 11_062d) were used for the comparison with the CO_2 sonde data obtained on 3 February. Figure 12 also shows the CONTRAIL 11_060d and 11_062d flight paths and the CO_2 sonde launched at Moriya on 31 January and 3 February 2011. On 31 January, the flight time of the CONTRAIL

11_060d over Narita airport and the launch time of the CO_2 sonde at Moriya were close to each other. The flight path of the CONTRAIL 11_062d data on 2 February 2011 was near to that of the CO_2 sonde on 3 February 2011 and both observations were conducted in the early afternoon. The CONTRAIL data referred in the present study were obtained using the Continuous CO_2 Measuring Equipment (CME) located onboard commercial airliners (Machida et al. 2008; Matsueda et al. 2008). The typical measurement uncertainty (1σ) of the CME has been reported to be 0.2 ppm (Machida et al. 2008).

Figure 13 shows the vertical profiles of CO_2 observed by the CO_2 sonde at Moriya, the chartered aircraft at Kumagaya and Tsukuba, and the CONTRAIL over Narita airport on 31 January, 2011. The overall vertical distribution of the CO_2 sonde data was very similar with those of the chartered aircraft. The vertical profiles of the CONTRAIL 11_060d flight on 31 January at the 5.3–6.8 km altitude range were missing data because of the calibration period for the CME.

Figure 14 shows the comparison of CO_2 vertical profiles obtained by the CO_2 sonde over Moriya, NIES/JAXA chartered aircraft over Kumagaya and Tsukuba on 3 February 2011, and the CONTRAIL on 2 February 2011 over Narita. The vertical profile shape obtained by the chartered aircraft on 3 February resembled to that obtained by the CO_2 sonde, although the profile of chartered aircraft was shifted to the lower CO_2 concentration side compared with that of the CO2 sonde.

Table 2 lists the comparisons of the CO_2 concentrations measured by the balloon CO_2 sonde and NIES/JAXA chartered aircraft on 31 January and 3 February 2011. The averaged values of the aircraft measurement over the range of each balloon altitude ± 100 m are listed in Table 2, since the altitude resolution of the aircraft measurements are higher than that of the CO_2 sonde. For the measurements on 3 February, it is clear that the height

of the boundary layer around the altitude of 1 km is different between the CO_2 sonde and the NIES/JAXA aircraft measurements as shown in Figure 14. Therefore, the data below 1 km on 3 February are not included in Table 2. For the data on 31 January, the averaged value of the differences between the CO_2 sonde and the NIES/JAXA aircraft is small (0.42 ppm), which corresponds to the bias of the measurements. The standard deviation of the differences is 1.24 ppm. For the data on 3 February, the bias is large (1.41 ppm), while the standard deviation of the differences is not so large (1.00 ppm), which corresponds to the similar but shifted vertical profiles in shapes between the CO_2 sonde and aircraft measurements as shown in Figure 14. The difference between the CO_2 sonde data and NIES/JAXA chartered aircraft data on 3 February is nearly equal to the difference between CONTRAIL data on 2 February and NIES/JAXA chartered aircraft data on 3 February.

Table 3 lists the comparisons of the CO_2 concentrations measured by the balloon CO_2 sonde and CONTRAIL aircraft, 11_060d on 31 January and 11_06 on 2 February 2011 up to the altitude of 7000 m. The averaged values of the aircraft measurements over the range of each balloon altitude ± 200 m are listed in Table 3. The biases between the CO_2 sonde and the CONTRAIL aircraft results are small, 0.33 and 0.35 ppm, and the standard deviations of the differences are 1.16 and 1.30 ppm for the results on 31 January and 3 February, respectively.

From the comparison between the CO_2 sonde data and the aircrafts (NIES/JAXA and CONTRAIL) data, it was found that the CO_2 sonde observation is larger than those of aircrafts by about 0.6 ppm in average. The standard deviation of the difference from the CO_2 sonde and aircraft observations resulted in 1.2 ppm (1σ). Assuming that the 4 sets of aircraft measurement data obtained by the NIES/JAXA and CONTRAIL observations

were correct within the published uncertainties and ignoring differences in the flight time and geographical routes, the measurement error of the CO_2 sonde system was estimated from the standard deviations of all the difference values in Tables 2 and 3. The estimated error value up to the altitude of 7 km was 0.6±1.2 ppm for the CO_2 sonde observation with the 240 m altitude resolution and 3 m s^{-1} ascending speed. The root mean square value (1.3 ppm) from all the difference value in Table 2 and 3 means that the CO_2 sonde can measure CO_2 vertical profiles within 1.3 ppm on average compared to the aircraft observations.

According to the paper (Shirai et al. 2012), the paper reports that the one month mean value of SD in CO_2 mixing ratio over Narita airport in Japan by CONTRAIL CO_2 vertical profile observations. The one month mean value of the SD in CO_2 mixing ratio over Narita at Planetary Boundary Layer (PBL) are 2.67ppm in January and 3.73ppm in February, respectively. Also, At the altitude of 5 km and 9 km over Narita, the one month mean value of the SD in CO_2 mixing ratio are 1.01ppm in January, 0.64ppm in February, and 0.73ppm, 0.64ppm, respectively. At the altitude of 5 km over Narita, the maximum difference is 9ppm in January and 5ppm in February.

Chapter 4

CO_2 sonde observations in various places

4.1. CO_2 sonde observations over a forested area

Figure 15 shows the vertical profiles of the CO_2 mixing ratio, temperature, and relative humidity obtained in the balloon-borne experiment of the CO_2 sonde at Moshiri (44.4°N, 142.3°E) on 26 August 2009. The launch site is located in rural area of Hokkaido, Japan, and is surrounded by forests. The CO_2 sonde was launched at 13:29 LST and ascended with a mean vertical speed of approximately 3 m s^{-1}. The CO_2 sonde reached an altitude of 10 km after 56 min. The wind horizontally transported the CO_2 sonde distances of 10 km and 21 km northeast when the CO_2 sonde reached altitudes of 5 km and 8 km, respectively. The CO_2 sonde rapidly moved 52 km southeast at an altitude of 16 km. Finally, the CO_2 sonde reached an altitude of 28 km before the balloon burst and the subsequent fall of the sonde was directed by the parachute into the Sea of Okhotsk located 80 km east of the launch site. The error bars for the CO_2 mixing ratio in Figure 15a were calculated from the deviation of the signal intensities from the CO_2 sensor during the 40-s measurement periods for the ambient air and the two standard gases.

Generally, along with the increase of the altitude, the temperature decreases. However, there are some inversion layers where the temperature increases with the altitude. The vertical temperature profile in Figure 15b indicated the existence of three inversion layers at altitudes of approximately 2.0, 3.2, and 4.3 km. The relative humidity from the ground to the first inversion layer at 2.0 km and between the second and third inversion layers from 3.2 to 4.3 km were higher as compared to those observed from 2.0 to 3.2 km and from 4.3 to 7.5 km. The CO_2 mixing ratio was the lowest near the ground (~373 ppm) and increased to approximately 384 ppm at an altitude of 4–5 km around the third

inversion layer before reaching a value of 387 ppm in the upper troposphere (5–9 km). The inversion layers suggest that the mixing of the air masses are not sufficient and that the upper and lower layers come from different areas where the CO_2 mixing ratios are different.

Significant decreases in the CO_2 mixing ratios were observed in the two lower layers from the ground to 3.2 km. Considering the clear weather on the day of the balloon experiment, these results can be explained by the uptake of CO_2 near the surface by plants in the forests through photosynthesis processes during daytime hours, and the diffusion and advection of the air mass containing low CO_2 concentrations toward upper altitudes.

Because the information of the CO_2 mixing ratio vertical profiles near the surface is critically important to estimate the flux around the observation point, the vertical profile data taken by our CO_2 sonde should be useful.

4.2. CO2 sonde observations over an urban area

Figure 16 shows the vertical profiles of the CO_2 mixing ratio, temperature, and relative humidity obtained by the CO_2 sonde at Moriya (35.93°N, 140.00°E) on 3 February 2011. The launching time was 13:10 LST and the sonde ascended with a mean vertical speed of approximately 2.9 m s^{-1}. Moriya is located in the Kanto region and is 40 km northeast of the Tokyo metropolitan area. The launching site was surrounded by heavy traffic roads and residential areas. As seen in Figure 16a, high values of CO_2 mixing ratio were observed from the ground up to an altitude of 1 km. The average CO_2 volume mixing ratio in this layer was higher than that measured in the free troposphere above by approximately 15 ppm. A small temperature inversion layer appeared at approximately 1 km and the maximum relative humidity was observed just below this inversion layer

(Figures 16b and c). These results suggested that the CO_2 emitted from anthropogenic sources in and/or around the Tokyo metropolitan area accumulated in the boundary layer at altitudes below 1 km.

When the small increase of a column XCO_2 value, for example, is observed by a satellite observation, it is difficult to estimate which part of the atmosphere is responsible for the increase of XCO_2, the boundary layer with strong CO_2 emission on the nearby area, or the free troposphere. Considering this fact, the vertical profile data obtained by the CO_2 sonde around urban areas should provide more useful information than the column averaged observations obtained by satellites and FTS measurements to estimate the flux of anthropogenic CO_2 emitted in and/or around urban areas.

Chapter 5

Application results of the CO_2 sonde

From the observation using the CO_2 sonde, CO_2 vertical profiles are obtained in various situations (Inai et al, 2018 and Nomura et al.2018). Figure 17 shows vertical profiles of CO_2, relative humidity (RH) (solid lines) and ozone (red solid line) and temperature (black dashed line), taken on 07 February 2012, 00:14 (UT) from R/V Hakuho Maru in the equatorial eastern Pacific, which is taken from Inai et al. (2018). In the pacific regions, the CO_2 vertical profiles were almost constant, since there were no local emissions nearby.

The GOSAT satellite observations cannot provide vertical profiles of CO2 but averaged mixing ratios of the total CO_2 column density (XCO_2). We have compared the column mixing ratios (XCO_2) derived from balloon-borne CO_2 measurement systems with the data obtained by the CO_2 monitoring satellite GOSAT on the same days. The balloons sondes were launched at the Moriya site, Ibaraki at around 13:00. The GOSAT data were measured above Tsukuba. Figure 18 shows two sets of data for the vertical profiles on Feb. 3 (upper) and Jan. 31, 2011 (lower) and plots of column densities XCO_2 derived from the profiles with GOSAT satellite data. On Feb. 3, in the boundary layer from ground to 1 km, the concentration of CO_2 is very high. Due to the slow wind speed, CO_2 emitted from local sources stagnated in the boundary layer. This day, the XCO_2 value of the GOSAT is also high. On the other hand, on January 31 the XCO_2 value of the GOSAT is smaller than the seasonal average curve. The lower part of figure 18 shows the CO_2 vertical profile on January 31. As can be seen in this figure, in the boundary layer, the concentration of CO_2 is not high. Due to the fast wind speed, CO_2 emitted from local sources did not stagnate in the boundary layer. Figure 19

indicates the schematic diagrams for the explanation of lower and higher values of GOSAT observation than the seasonal average curve, which are elucidated by the balloon-borne experiments. Table 4 listed the XCO_2 values derived from the balloon experiments and GOSAT observation values. The balloons sondes were launched at the Moriya site, Ibaraki at around 13:00. The GOSAT data were measured above Tsukuba. The averaged difference and standard deviations for the six balloon experiments and GOSAT XCO_2 data on the same day were -0.61±1.27.

Chapter 6

Conclusion

The CO_2 sonde has been shown to be a feasible instrument for CO_2 measurements in the troposphere. The laboratory test with a vacuum chamber has shown precision of the CO_2 sonde at ~1010 hPa for 0.6 ppm and at ~250 hPa for 1.2 ppm. The comparisons of the CO_2 vertical profiles obtained by the CO_2 sonde with two kinds of aircraft observations, the CONTRAIL and the NIES/JAXA chartered aircraft, were also performed. The CO_2 sonde and CONTRAIL data were consistent. The CO_2 sonde data on 31 January 2011 was in good agreement with chartered aircraft data on the same day, but the CO_2 sonde data on 3 February 2011 was larger by approximately 1.4 ppm compared with the chartered aircraft data obtained on the same day from the ground to an altitude of 7 km. The measurement errors of the CO_2 sonde system up to the altitude of 7 km were estimated to be 1.4 ppm for a single point of 80-s period measurements in this flight. We use the 20 seconds for each calibration gases measurement data and 40 seconds for the ambient air measurement data.

We conducted field CO_2 sonde observations in Japan and successfully obtained CO_2 vertical profiles from the ground up to altitudes of approximately 10 km. The CO_2 sonde cached a positive gradient in the CO_2 mixing ratio with increasing altitude from the ground to 4 km altitude over Moshiri on 26 August 2009. The lower CO_2 mixing ratios in the boundary layer were likely caused by photosynthesis in plants in the forested area around the launch site. In contrast, higher concentrations of CO_2 due to the anthropogenic emissions of CO_2 in and/or around the Tokyo metropolitan area were captured in the boundary layer in the observation over Moriya on 3 February 2011.

Our results showed that low-cost CO_2 sondes could potentially be used to frequently measure vertical profiles of CO_2 in many places in the world providing as useful information for better understanding of global and regional carbon budgets by replenishing the present sparse observation coverage. Also, the CO_2 sonde observation data will help improve inter-comparison exercise for inverse models as well as for the partial validation of satellite column integral data. In the future, the CO_2 sonde data will be used for the validation of satellites and the calibration of ground-based observations of sunlight spectroscopic measurements for column values of CO_2 concentration.

References

Ahmadov, R., C. Gerbig, R. Kretschmer, S. Körner, C. Rödenbeck, P. Bousquet, and M. Ramonet, 2009: Comparing high resolution WRF-VPRM simulation and two global CO_2 transport models with coastal tower measurements of CO_2, *Biogeosciences*, **6**, 807–817, doi:10.5194/bg-6-807-2009.

Andrews, A. E. and Coauthors, 2014: CO_2, CO, and CH_4 measurements from tall towers in the NOAA Earth System Research Laboratory's Global Greenhouse Gas Reference Network: instrumentation, uncertainty analysis, and recommendations for future high-accuracy greenhouse gas monitoring efforts, *Atmos. Meas. Tech.*, **7**, 647-687, doi:10.5194/amt-7-647-2014.

Baker, D. F. and Coauthors, 2006: TransCom 3 inversion intercomparison: Impact of transport model errors on the interannual variability of regional CO_2 fluxes, 1988–2003, *Global Biogeochem. Cycles*, **20**, GB1002, doi:10.1029/2004GB002439.

Bakwin, P. S., P. P. Tans, C. Zhao, W. Ussler III, and E. Quesnell, 2002: Measurements of carbon dioxide on a very tall tower, *Tellus* **47B**, 535-549, 1995, doi:10.1034/j.1600-0889.47.issue5.2.x.

Battle, M., M. L. Bender, P. P. Tans, J. W. C. White, J. T. Ellis, T. Conway, and R. J. Francey, Global carbon sinks and their variability inferred from atmospheric O_2 and $\delta^{13}C$, Science, 287, 2467–2470, 2000.

Chédin, A., S. Serrar, R. Armante, N. A. Scott and A. Hollingsworth, 2002: Signatures of annual and seasonal variations of CO_2 and other greenhouse gases from comparisons between NOAA TOVS observations and radiation model simulations, *J. Climate,* **15**, 95-116, doi:10.1175/1520-0442(2002)015<0095:SOAASV>2.0.CO;2.

Conway, T. J., P. Tans, L. S. Waterman, K. W. Thoning, K. A. Masarie, and R. H.

Gammon, 1988: Atmospheric carbon dioxide measurements in the remote global troposphere, 1981–1984, *Tellus B*, **40**, 81–115, doi:10.1111/j.1600-0889.1988.tb00214.x.

Conway, T. J., P. P. Tans, L. S. Waterman, K. W. Thoning, D. R. Kitzis, K. A. Masarie, and N. Zhang, 1994: Evidence for interannual variability of the carbon cycle from the National Oceanic and Atmospheric Administration/Climate Monitoring and Diagnostics Laboratory global air sampling network, *J. Geophys. Res.*, **99**(D11), 22,831–22,855, doi:10.1029/94JD01951.

Crevoisier, C., S. Heilliette, A. Chédin, S. Serrar, R. Armante, and N. A. Scott, 2004: Midtropospheric CO_2 concentration retrieval from AIRS observations in the tropics, *Geophys*. *Res*. *Let*., **31**, L17106, doi:10.1029/2004GL020141.

Daube, B. C., K. A. Boering, A. E. Andrews, and S. C. Wofsy, 2002: A high-precision fast-response airborne CO_2 analyzer for in situ sampling from the surface to the middle stratosphere, *J. Atmospheric Ocean. Technol*., **19**(10), 1532-1543, doi:10.1175/1520-0426(2002)019 <1532:AHPFRA>2.0.CO;2.

Dils, B. and Coauthors, 2006: Comparisons between SCIAMACHY and ground-based FTIR data for total columns of CO, CH_4, CO_2 and N_2O, *Atmos. Chem. Phys.,* **6**, 1953–1976, doi:10.5194/acp-6-1953-2006.

Durry, G., N. Amarouche, V. Zéninari, B. Parvitte, T. Lebarbu, and J. Ovarlez, 2004: In situ sensing of the middle atmosphere with balloon borne near-infrared laser diodes, *Spectrochimica Acta Part A,* **60**, 3371–3379, doi:10.1016/j.saa.2003.11.050.

Eldering, A. and Coauthors, 2017: The Orbiting Carbon Observatory-2: first 18 months of science data products, *Atmos. Meas. Tech.*, **10**, 549-563, doi:10.5194/amt-10-549-2017.

ESA (Europian Space Agency), Image Gallery Carbon Dioxide, http://www.esa-ghg-cci.org/?q=node/115

Gurney, K. R. and Coauthors, 2002: Towards robust regional estimates of CO_2 sources and sinks using atmospheric transport models, *Nature,* **415**, 626-630, doi:10.1038/415626a.

Gurney, K. R. and Coauthors, 2004: Transcom 3 inversion intercomparison: Model mean results for the estimation of seasonal carbon sources and sinks. *Global Biogeochem. Cycles,* **18**, GB1010, doi:10.1029/2003GB002111.

Ghysels, M., G. Durry, N. Amarouche, J. Cousin, L. Joly, E. D. Riviere, and L. Beaumont, 2012: A lightweight balloon-borne laser diode sensor for the in-situ measurement of CO_2 at 2.68 micron in the upper troposphere and the lower stratosphere, *Appl. Phys. B*, **107**(1), 213-220, doi:10.1007/s00340-012-4887-y.

Inai,Y., S. Aoki, H. Honda, H. Furutani, Y. Matsumi, M. Ouchi, S. Sugawara, F. Hasebe, M. Uematsu, M. Fujiwara, 2018: Balloon-borne tropospheric CO2 observations over the equatorial eastern and western Pacific, *Atmospheric Environment*, vol 184, 24-36, https://doi.org/10.1016/j.atmosenv.2018.04.016

Inoue, H. Y., and H. Matsueda, 2001: Measurements of atmospheric CO_2 from a meteorological tower in Tsukuba, Japan. *Tellus,* **53B**, 205–219, doi:10.1034/j.1600-0889.2001.01163.x.

IPCC (Intergovernmental Panel on Climate Change), Climate change 2013, http://www.ipcc.ch/report/ar5/index.shtml

Joly. L., B. Parvitte, V. Zeninari, and G. Durry, 2007: Development of a compact CO_2 sensor open to the atmosphere and based on near-infrared laser technology at 2.68 μm, *Appl. Phys. B*, **86**, 743–748, doi:10.1007/s00340-006-2568-4.

Karion, A., C. Sweeney, P. Tans, and T. Newberger, 2010: AirCore: An innovative atmospheric sampling system, *J. Atmos. Oceanic Technol.,* **27**, 1839–1853, doi:10.1175/2010JTECHA1448.1.

Komhyr, W. D., T. B. Harris, L. S. Waterman, J. F. S. Chin, and K. W. Thoning, 1989: Atmospheric carbon dioxide at Mauna Loa Observatory 1. NOAA global monitoring for climatic change measurements with a nondispersive infrared analyzer, 1974–1985, *J. Geophys. Res.*, **94**, 8533–8547, doi:10.1029/JD094iD06p08533.

Machida, T., H. Matsueda, Y. Sawa, Y. Nakagawa, K. Hirotani, N. Kondo, K. Goto, K. Ishikawa, T. Nakazawa, and T. Ogawa, 2008: Worldwide measurements of atmospheric CO_2 and other trace gas species using commercial airlines, *J. Atmos. Oceanic Technol.*, **25**(10), 1744–1754, doi:10.1175/2008JTECHA1082.1.

Maksyutov, S., K. Nikolay, Y. Nakatsuka, P. K. Patra, T. Nakazawa, T. Yokota, and G. Inoue, 2008: Projected Impact of the GOSAT observations on regional CO_2 flux estimations as a function of total retrieval error. *J. Remote Sensing Soc. Japan*, **28**, 190-197, doi:10.11440/rssj.28.190.

Manning, AC, Keeling RF. 2006: Global oceanic and land biotic carbon sinks from the Scripps atmospheric oxygen flask sampling network. *Tellus Series B-Chemical and Physical Meteorology*. **58**, 95-116.

Matsueda, H., T. Machida, Y. Sawa, Y. Nakagawa, K. Hirotani, H. Ikeda, N. Kondo, and K. Goto, 2008: Evaluation of atmospheric CO_2 measurements from new flask air sampling of JAL airliner observations. *Pap. Meteor. Geophys.*, **59**, 1–17, doi:10.2467/mripapers.59.1.

Morino, I. and Coauthors, 2011: Preliminary validation of column-averaged volume mixing ratios of carbon dioxide and methane retrieved from GOSAT short-

wavelength infrared spectra, Atmos. Meas. Tech., **4**, 1061–1076, doi:10.5194/amt-4-1061-2011.

Nakazawa, T., S. Murayama, K. Miyashita, S. Aoki, and M. Tanaka, 1992: Longitudinally different variations of lower tropospheric carbon dioxide concentrations over the North Pacific Ocean, *Tellus*, **44B**, 161–172, doi:10.3402/tellusb.v44i3.15438.

Nakazawa, T., T. Machida, S. Sugawara, S. Murayama, S. Morimoto, G. Hashida, H. Honda, and T. Itoh, 1995: Measurements of the stratospheric carbon dioxide concentration over Japan using a balloon-borne cryogenic sampler, *Geophys. Res. Letter,* **22**, 1229–1232, doi:10.1029/95GL01188.

Nomura, S., H. Mukai, Y. Terao, K. Takagi, M. Mohamad, and M Firdaus Jahaya, 2018: Evaluation of forest CO_2 fluxes from sonde measurements in three different climatological areas including Borneo, Malaysia, and Iriomote and Hokkaido, Japan, *Tellus B: Chemical and Physical Meteorology,* 70:1, 1-19, doi:10.1080/16000889.2018.1426316

Pales, J. C., and C. D. Keeling, 1965: The concentration of atmospheric carbon dioxide in Hawaii, *J. Geophys. Res*., **70**(24), 6053-6076, doi:10.1029/JZ070i024p06053.

Shirai, T. et al. 2012: Relative contribution of transport/surface flux to the seasonal vertical synoptic CO2 variability in the troposphere over Narita, *Tellus B*, **64**, 19138, http://dx.doi.org/10.3402/tellusb.v64i0.19138

Stephens, B. B. and Coauthors, 2007: Weak northern and strong tropical land carbon uptake from vertical profiles of atmospheric CO_2, *Science*, **316**, 1732–1735, doi:10.1126/science.1137004.

Sweeney, C. and Coauthors, 2014: Seasonal climatology of CO_2 across North America

from aircraft measurements in the NOAA/ESRL Global Greenhouse Gas Reference Network, *J. Geophys. Res.,* **120**, 5155-5190, doi:10.1002/2014JD022591.

Tanaka, M., T. Nakazawa, and S. Aoki, 1983: High quality measurements of the concentration of atmospheric carbon dioxide. *J. Meteor. Soc. Japan*, **61**, 678-685, doi:10.2151/jmsj1965.61.4_678.

Tanaka, M., T. Nakazawa, and S. Aoki, 1987: Time and space variations of tropospheric carbon dioxide over Japan, *Tellus*, **39B**, 3–12, doi:10.3402/tellusb.v39i1-2.15318.

Tanaka, T., Y. Miyamoto, I. Morino, T. Machida, T. Nagahama, Y. Sawa, H. Matsueda, D. Wunch, S. Kawakami, and O. Uchino, 2012: Aircraft measurements of carbon dioxide and methane for the calibration of ground-based high-resolution Fourier Transform Spectrometers and a comparison to GOSAT data measured over Tsukuba and Moshiri. *Atmos. Meas. Tech.,* **5**, 2003–2012, doi:10.5194/amt-5-2003-2012.

Tans, P. P., T. Conway, and T. Nakazawa, 1989: Latitudinal distribution of the sources and sinks of atmospheric carbon dioxide derived from surface observations and an Atmospheric Transport Model, *J. Geophys. Res.*, **94**, 5151–5172, doi:10.1029/JD094iD04p05151.

Watai, T., T. Machida, N. Ishizaki, and G. Inoue, 2006: A lightweight observation system for atmospheric carbon dioxide concentration using a small unmanned aerial vehicle. *J. Atmos. Oceanic Technol.,* **23**, 700–710 doi:10.1175/JTECH1866.1.

Winderlich, J., H. Chen, C. Gerbig, T. Seifert, O. Kolle, J. V. Lavrič, C. Kaiser, A. Höfer, and M. Heimann, 2010: Continuous low-maintenance CO_2/CH_4/H_2O measurements at the Zotino Tall Tower Observatory (ZOTTO) in Central Siberia, *Atmos. Meas. Tech.,* **3**, 1113–1128, doi:10.5194/amt-3-1113-2010.

WMO, 2016: The state of greenhouse gases in the atmosphere using global observations

through 2015, *WMO Greenhouse Gas Bull.,* **12**, 1–8.

Wofsy, S. C., the HIPPO science team and cooperating modellers and satellite teams, 2011: HIAPER Pole-to-Pole Observations (HIPPO): fine-grained, global-scale measurements of climatically important atmospheric gases and aerosols, *Phil. Trans. R. Soc. A*, **369**, 2073–2086, doi:10.1098/rsta.2010.0313.

Wunch, D., G. C. Toon, J. L. Blavier, R. A. Washenfelder, J. Notholt, B. J. Connor, D. W. T. Griffith, V. Sherlock, and P. O. Wennberg, 2011: The Total Carbon Column Observing Network. *Phil. Trans. R. Soc. A,* **369**, 2087–2112, doi:10.1098/rsta.2010.0240.

Yokota, T., Y. Yoshida, N. Eguchi, Y. Ota, T. Tanaka, H. Watanabe, and S. Maksyutov, 2009: Global concentrations of CO_2 and CH_4 retrieved from GOSAT: First preliminary results, *Sci. Online Lett. Atmos.*, **5**, 160–163, doi:10.2151/sola.2009–041.

Yoshida, Y., Y. Ota, N. Eguchi, N. Kikuchi, K. Nobuta, H. Tran, I. Morino, and T. Yokota, 2011: Retrieval algorithm for CO_2 and CH_4 column abundances from short-wavelength infrared spectral observations by the Greenhouse gases observing satellite, *Atmos. Meas. Tech*., **4**, 717–734, doi:10.5194/amt-4-717-2011.

Tables and figures

Table 1. CONTAIL flight data near to the CO_2 sonde measurements on 31 January and 3 February 2011.

Data set name	Date	Time (LST)[a]
11_057a	CONTRAIL (29 January)	19:01
11_058d	CONTRAIL (30 January)	15:06
11_059a	CONTRAIL (30 January)	18:46
11_060d	CONTRAIL (31 January)	15:07
11_061a	CONTRAIL (1 February)	18:46
11_062d	CONTRAIL (2 February)	14:58
11_063a	CONTRAIL (4 February)	18:58
	CO_2 sonde (31 January)	13:06
	CO_2 sonde (3 February)	13:10

[a] Time for the CONTRAIL data represents the flight time in Japan Standard Time at an altitude of 1 km over the Narita airport. Time for the CO_2 sonde data represents the launching time at Moriya.

Table 2. Comparisons of the CO_2 concentrations between the balloon CO_2 sonde and NIES/JAXA chartered aircraft measurements on 31 January and 3 February 2011.

JAXA-NIES Chartered Aircraft (31 January 2011)				JAXA-NIES Chartered Aircraft (3 February 2011)			
Altitude (m)[a]	Balloon CO_2 (ppm)	Aircraft CO_2 (ppm)[b]	Difference (ppm)[c]	Altitude (m)[a]	Balloon CO_2 (ppm)	Aircraft CO_2 (ppm)[b]	Difference (ppm)[c]
849	399.05	397.62	1.43	1324	396.60	394.45	2.15
1202	398.16	397.53	0.63	1612	394.65	393.03	1.62
1610	398.00	397.17	0.83	1917	394.86	394.10	0.76
2038	396.50	396.95	-0.45	2223	395.77	393.54	2.23
2291	398.03	396.04	1.99	2539	395.41	393.95	1.45
2463	396.54	395.65	0.89	2867	394.71	395.11	-0.40
2844	393.44	395.24	-1.79	3215	394.99	392.99	2.00
3329	395.45	394.15	1.30	3543	393.59	393.07	0.52
3732	393.51	393.63	-0.12	3764	393.69	393.40	0.28
4161	395.47	393.54	1.93	3938	395.15	393.11	2.04
4575	394.62	392.94	1.68	4169	393.83	392.68	1.15
4918	393.24	393.64	-0.41	4458	396.57	393.51	3.06
5273	392.41	393.25	-0.84	4750	394.88	393.69	1.19
5654	393.02	393.47	-0.45	5047	396.53	394.01	2.53
6083	391.87	392.91	-1.04	5214	395.91	393.45	2.46
6510	392.76	391.65	1.11	5383	396.78	393.58	3.20
		Average =	0.42	5565	395.83	393.67	2.15
		Std Dev[d] =	1.16	5781	395.18	393.39	1.80
		RMS[e] =	1.20	6092	391.75	392.83	-1.09
				6287	392.44	392.42	0.02
				6467	393.67	392.23	1.44
				6639	395.07	392.42	2.65
				6815	394.00	393.00	1.00
						Average =	1.41
						Std Dev[d] =	1.00
						RMS[e] =	1.62

a. Altitudes of the balloon-borne experiments using the in-flight calibration with 40-s time intervals.

b. Averaged values of the aircraft measurement results over the range of the balloon altitudes ± 100 m.

c. Difference values of [balloon CO_2] - [Aircraft CO_2]

d. Standard deviation of the differences (1σ).

e. Root mean square values.

Table 3. Comparisons of the CO_2 concentrations between the balloon CO_2 sonde measurements on 31 January and CONTRAIL aircraft CME on 31 January (11_06d) and between the CO_2 sonde on 3 February and CONTRAIL on 2 February (11_062d) up to the altitude of 7 km. The annotations are same as Table 1.

CONTRAIL 11_060d (31 January 2011)				CONTRAIL 11_062d (2 February 2011)			
Altitude (m)	Balloon CO_2 (ppm)	Aircraft CO_2 (ppm)	Difference (ppm)	Altitude (m)	Balloon CO_2 (ppm)	Aircraft CO_2 (ppm)	Difference (ppm)
849	399.05	398.21	0.84	1917	394.86	396.59	-1.73
1202	398.16	399.56	-1.40	2223	395.77	396.45	-0.68
1610	398.00	398.77	-0.76	2539	395.41	395.71	-0.30
2038	396.50	397.07	-0.57	2867	394.71	394.67	0.04
2291	398.03	395.97	2.06	3215	394.99	393.34	1.65
2463	396.54	394.55	1.99	3543	393.59	394.25	-0.66
2844	393.44	393.41	0.04	3764	393.69	394.33	-0.64
3329	395.45	394.25	1.20	3938	395.15	394.69	0.46
3732	393.51	393.58	-0.07	4458	396.57	394.09	2.48
4161	395.47	393.86	1.61	4750	394.88	395.02	-0.14
4575	394.62	393.18	1.44	5047	396.53	396.55	-0.01
4918	393.24	393.62	-0.38	5214	395.91	396.01	-0.10
5273	392.41	392.76	-0.35	5383	396.78	394.78	2.00
6866	392.31	393.26	-0.96	5565	395.83	393.69	2.14
		Average =	0.33	5781	395.18	393.79	1.39
		Std Dev =	1.16	6092	391.75	393.57	-1.82
		RMS =	1.17	6287	392.44	393.32	-0.88
				6467	393.67	392.89	0.78
				6639	395.07	392.84	2.23
				6815	394.00	393.11	0.90
						Average =	0.35
						Std Dev =	1.30
						RMS =	1.31

Table 4. Comparison of the column mixing ratios derived from balloon-borne CO_2 measurement systems with the same day data obtained by the CO_2 monitoring satellite GOSAT. The balloons sondes were launched at the Moriya site, Ibaraki at around 13:00. The GOSAT data were measured above Tsukuba.

Date	Balloon	GOSAT(Ver. 2)	GOSAT-Balloon
Dec. 22, 2009	**390.43**	**389.59**	**-0.84**
Jan. 31, 2011	**391.57**	**390.26**	**-1.31**
Feb. 3, 2011	**394.61**	**393.71**	**-0.90**
Jun. 30, 2012	**391.63**	**393.47**	**1.84**
Jan.08, 2013	**397.80**	**396.97**	**-1.83**
Average ± σ			**-0.61±1.27**

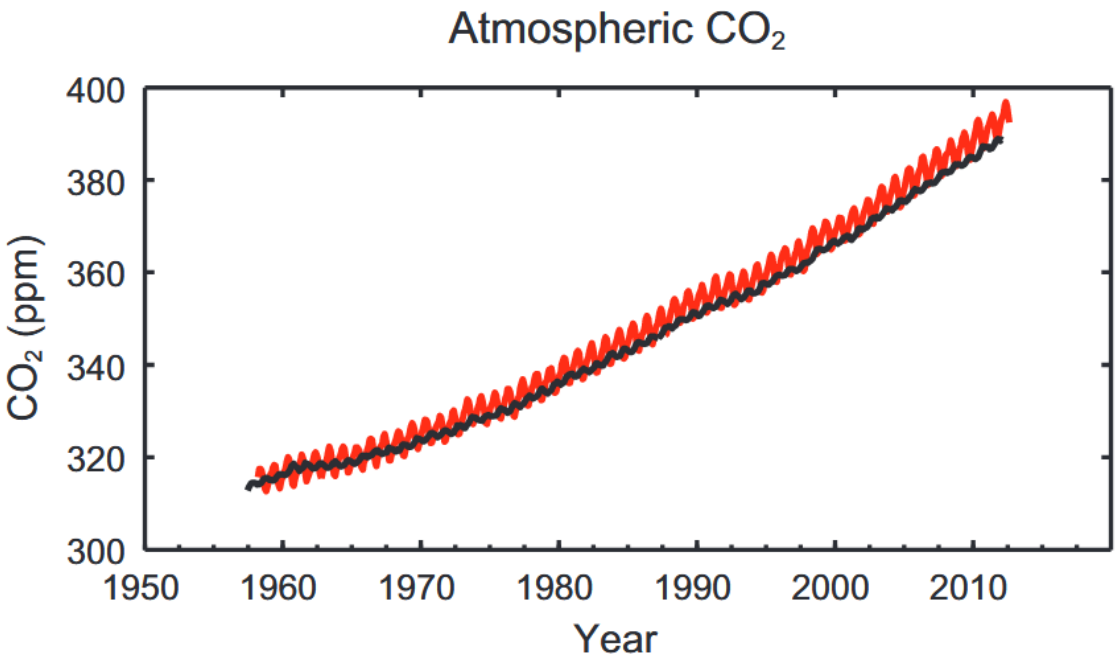

Figure 1. Multiple observed indicators of a changing global carbon cycle: atmospheric concentrations of carbon dioxide (CO_2) from Mauna Loa (19°32'N, 155°34'W – red) and South Pole (89°59'S, 24°48'W – black) since 1958 (IPCC, 2013).

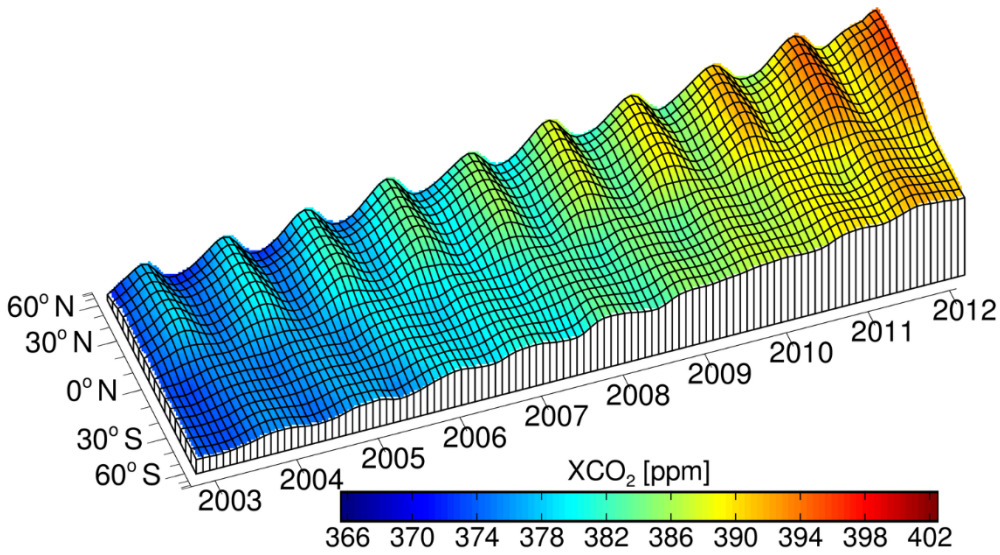

Figure 2. CO_2 "flying carpet" showing the CO_2 distribution as a function of time and latitude. The data have been retrieved from SCIAMACHY on ENVISAT.

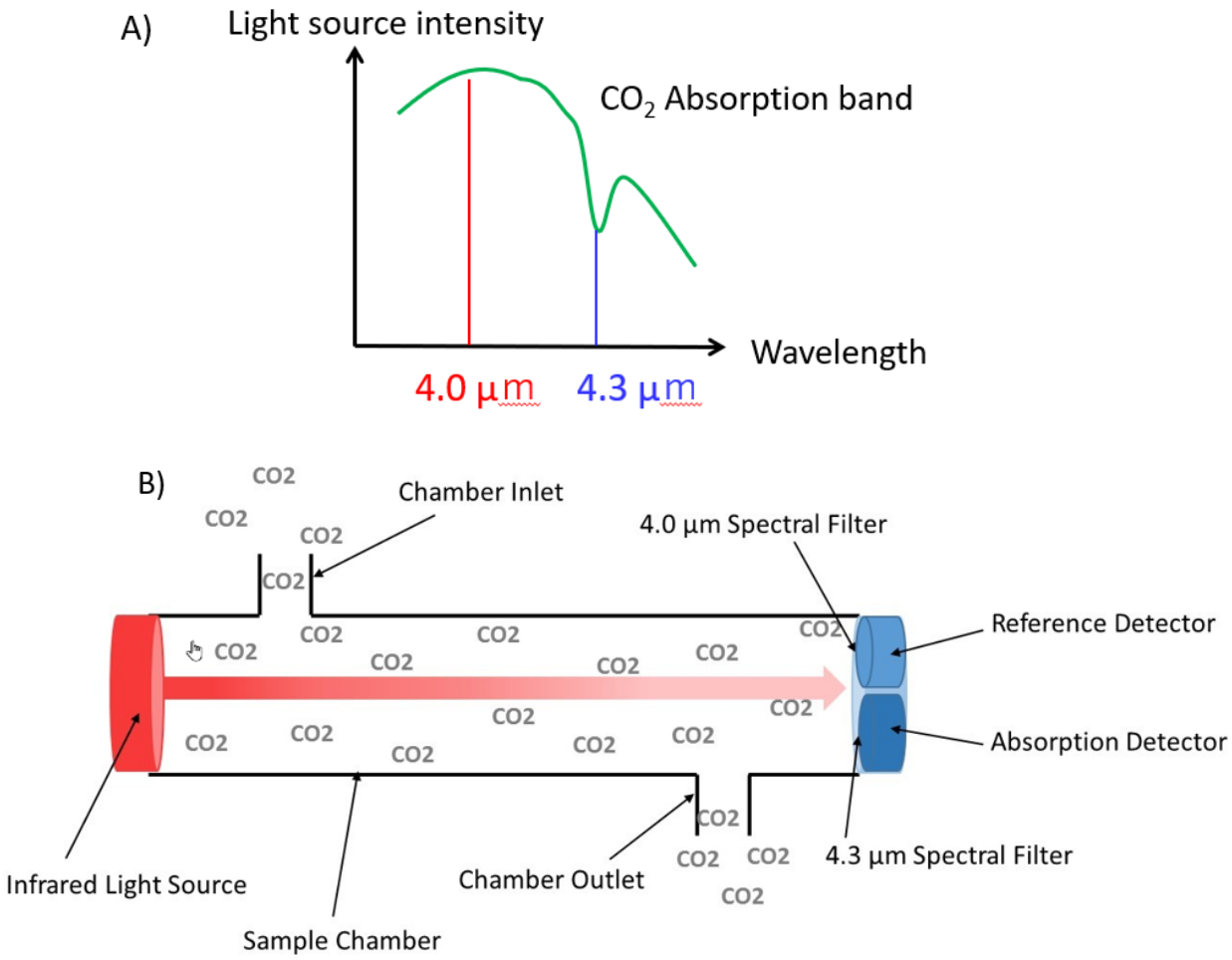

Figure 3. Schematic diagrams of the Non-Dispersive Infrared Detector (NDIR) technique for the measurement of atmospheric CO_2 concentrations. A) Absorption spectra of CO_2 and B) structural drawing of the NDIR instrument.

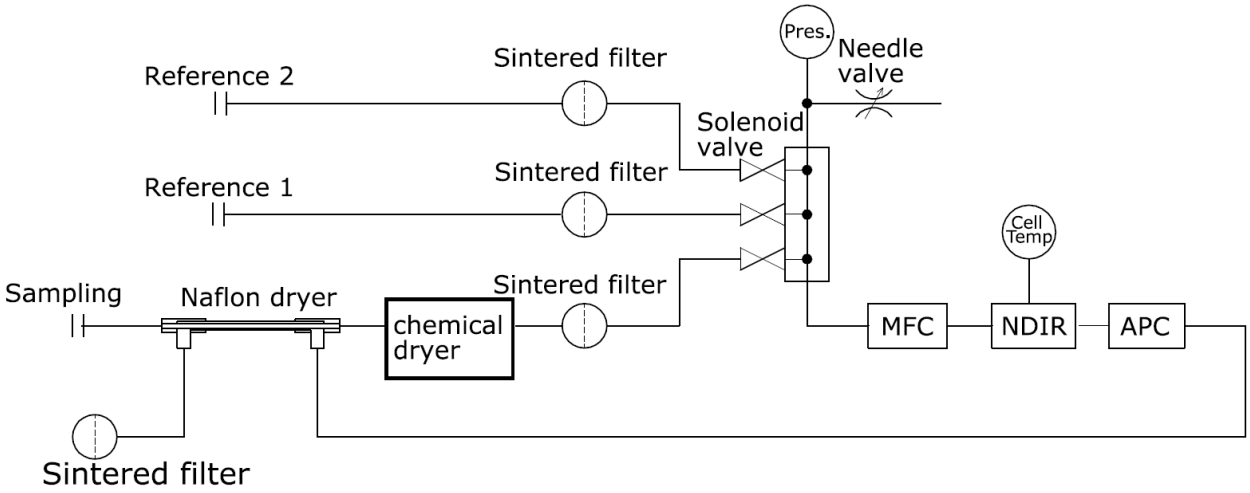

Figure 4. Schematic diagram of the NDIR measurement system. MFC: mass flow controller, and APC: automatic pressure controller.

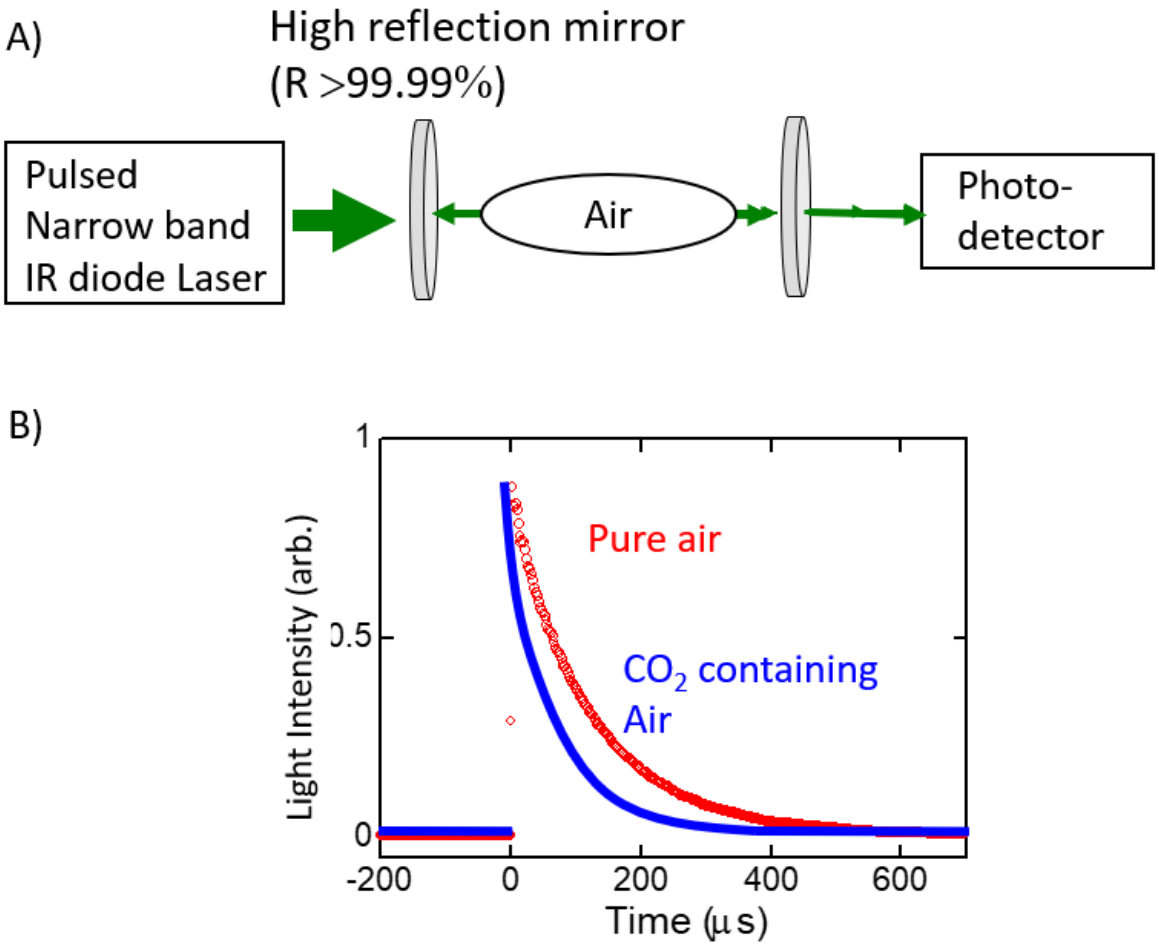

Figure 5. Schematic diagrams of the CO_2 Cavity Ring-Down Spectroscopy technique. A) structural drawing of the NDIR instrument and B) time profiles of the detector signals in the NDIR instrument. From the measurements of the decay rates the concentrations of CO_2 in the air can be derived.

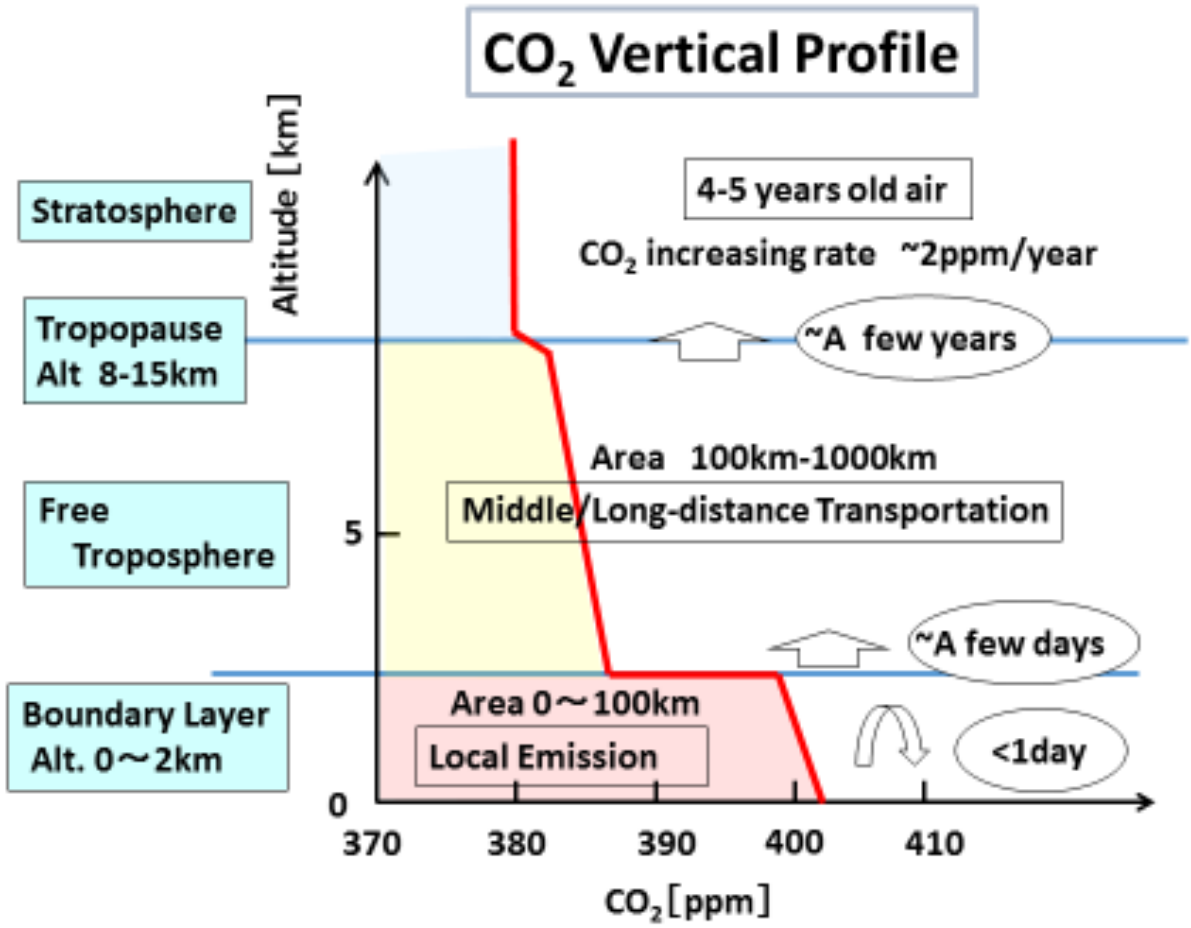

Figure 6. Schematic diagram of the CO_2 vertical profile in the troposphere.

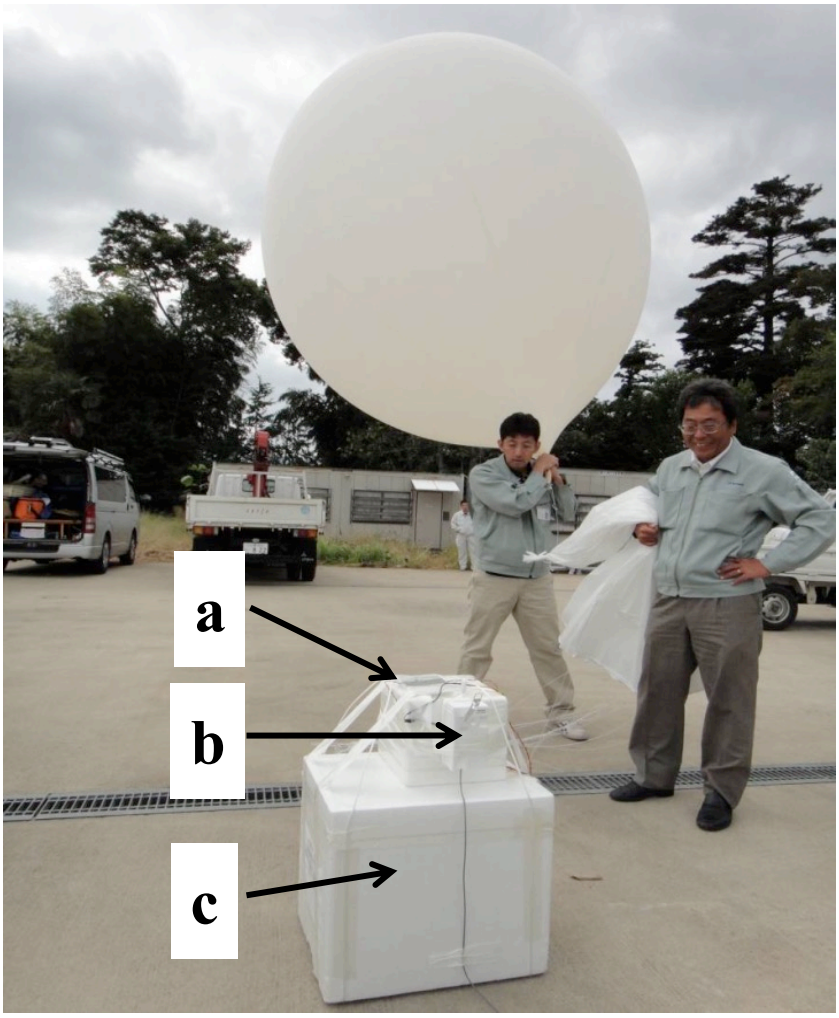

Figure 7. A photograph of the CO_2 sonde developed in this study before launching. a. CO_2 measurement package, b. GPS sonde, and c. Calibration gas package. The size of the CO_2 measurement package and the calibration gas package are width (W) 280 mm × height (H) 150 mm × depth (D) 280 mm and W 400 mm × H 420 mm × D 490 mm, respectively. The total weight of the CO_2 sonde (a + b + c) is 1700 g.

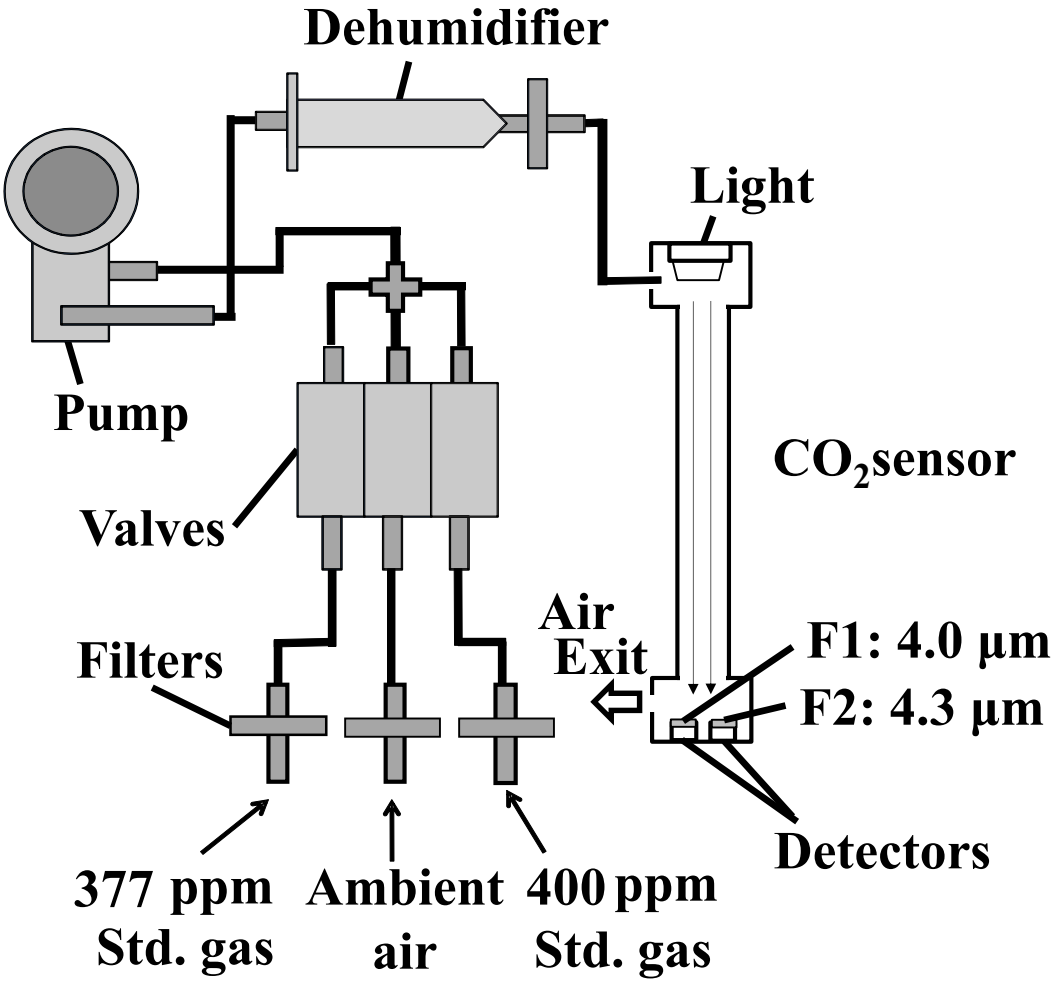

Figure 8. Schematic diagram of the CO_2 measurement package, where F1 and F2 represent the band-pass filters at wavelengths of 4.0 µm and 4.3 µm, respectively. The outlet port of the CO_2 sensor is open to ambient air. Details of the system are described in the text.

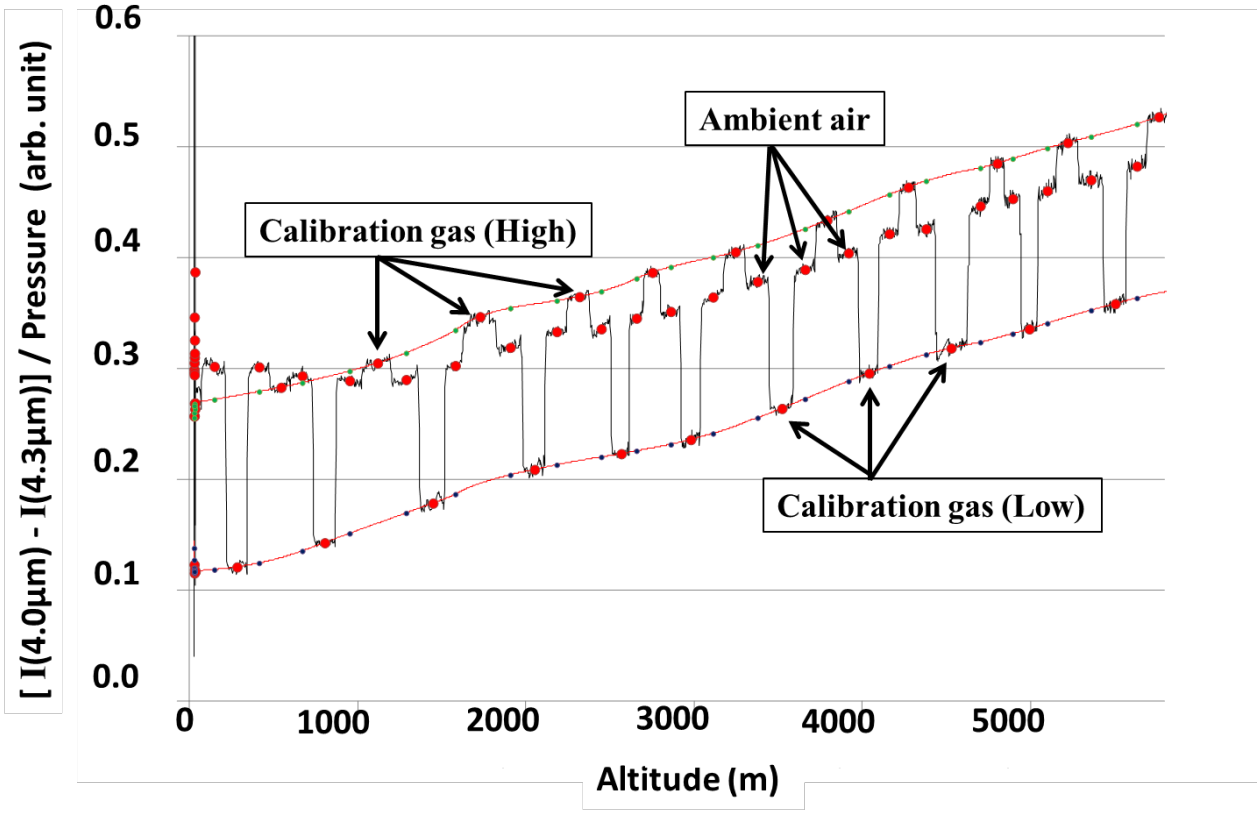

Figure 9. Raw data obtained by the CO_2 sonde launched on 26 September 2011 at Moriya, Japan. The vertical axis is difference between the 4.0 μm and 4.3 μm signal intensities divided by the ambient pressure.

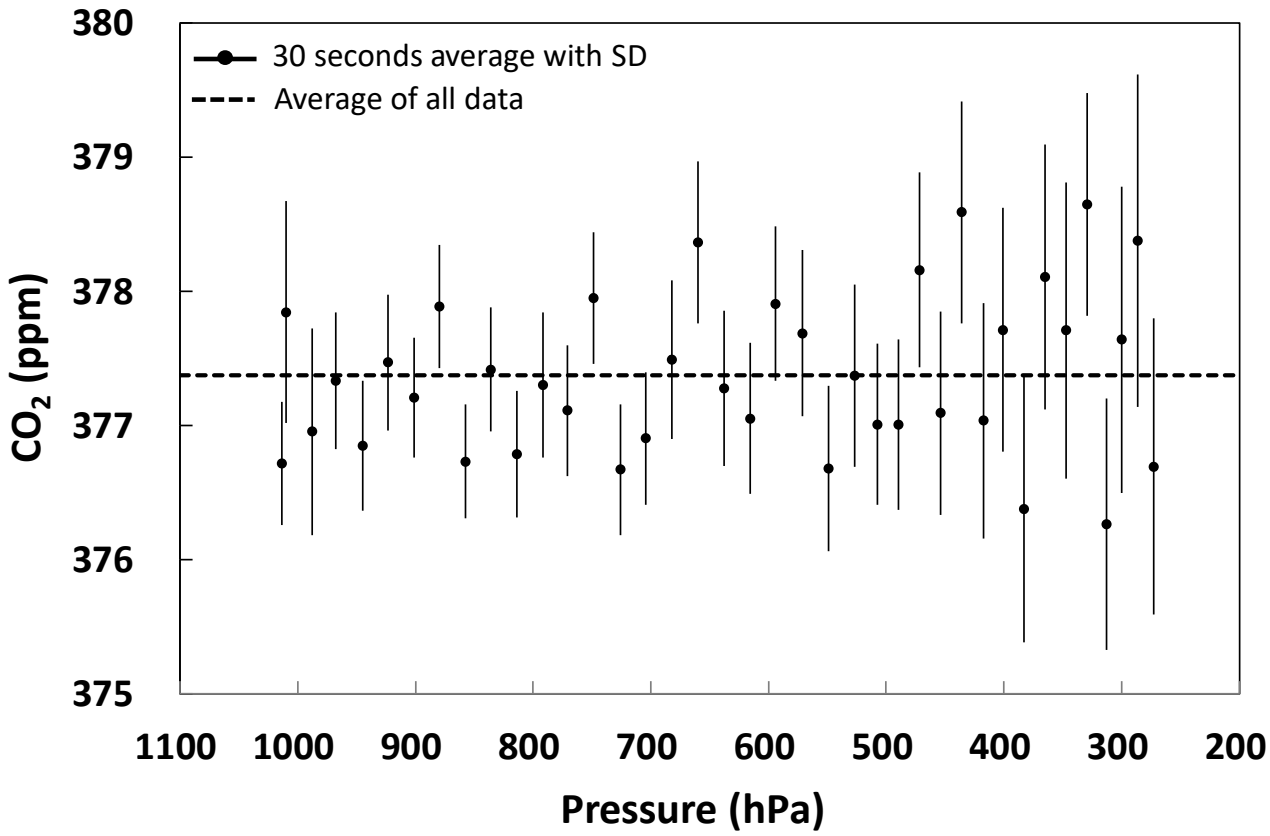

Figure 10. Results of a chamber experiment of the CO_2 sonde. Pressure in the chamber was changed from 1010 hPa (ground level pressure) to 250 hPa (about 10 km altitude pressure) at temperature about 298 K. The black circle and bar represent 30 second average value of CO_2 mixing ratio in the intermediate concentration gas package and standard deviation (SD), respectively. The black dashed line shows an average of all 30 second averaged values. See the text for more details.

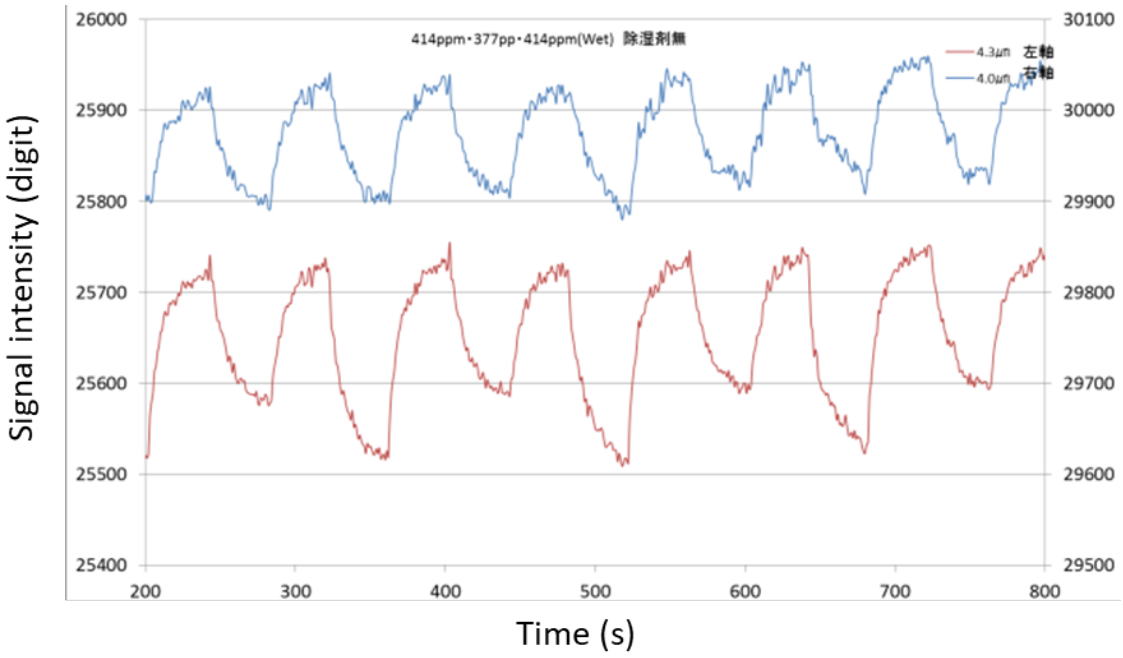

Figure 11. The signal intensities of 4.0 μm and 4.3 μm when the ambient air with water vapor passed through the CO_2 sensor in the CO_2 sonde.

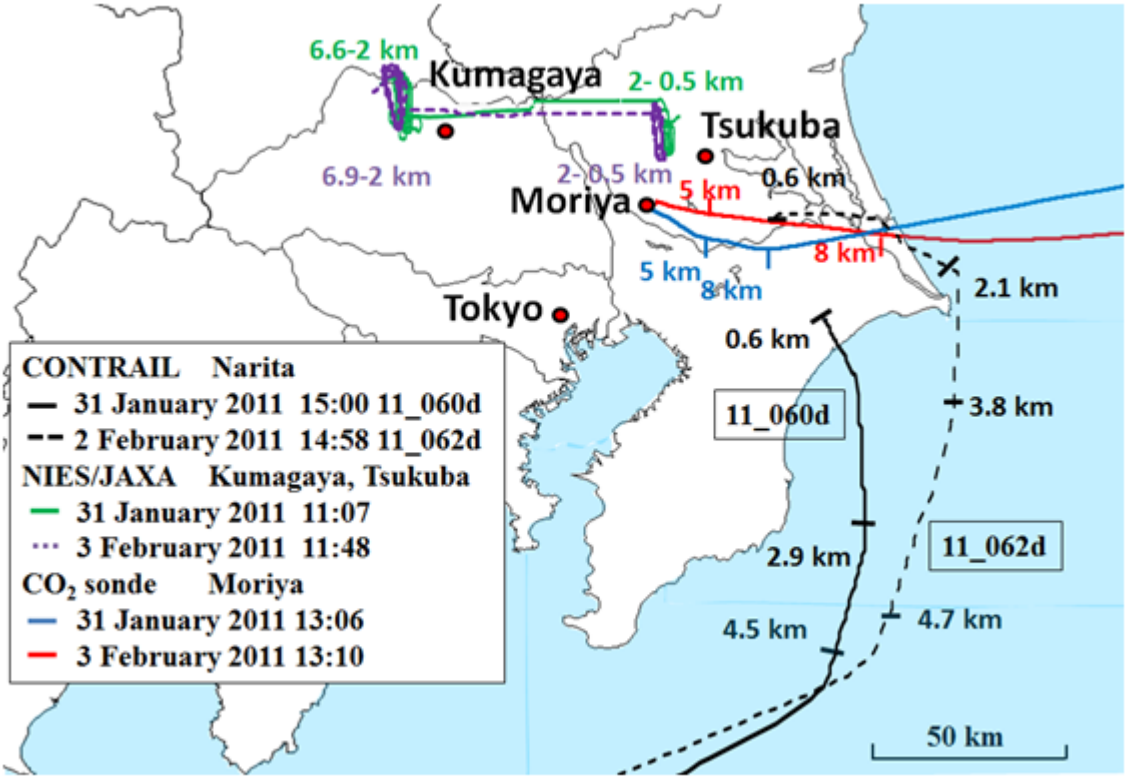

Figure 12. Flight paths of the CO_2 sonde observations launched at Moriya on 31 January (blue solid line) and 3 February (red solid line), the CONTRAIL 11_060d data on 31 January 2011 (black solid line) and 11_062d data on 2 February 2011 (black dashed line) from Hong Kong to Narita, and the NIES/JAXA chartered aircraft experiment on 31 January (green solid line) and 3 February (purple dotted line). The altitudes of the flight paths are indicated in the figure.

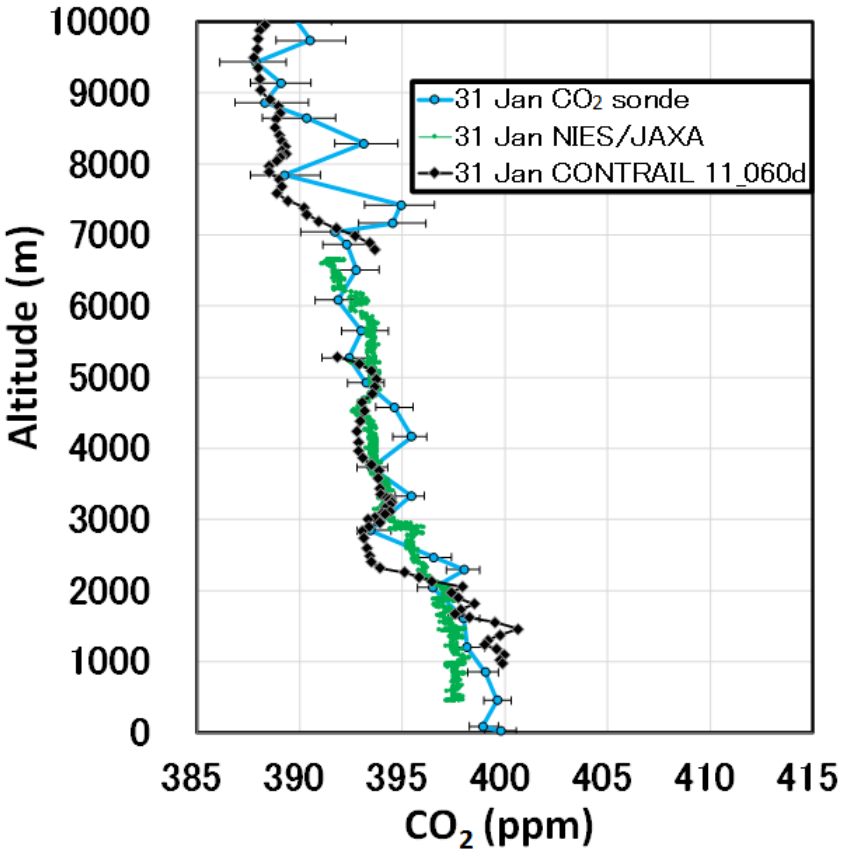

Figure 13. The CO_2 vertical profiles obtained by the CO_2 sonde (circles connected with blue lines), NIES/JAXA chartered aircraft data (dots connected with green lines), and the CONTRAIL data (diamonds connected with black lines) on 31 January 2011.

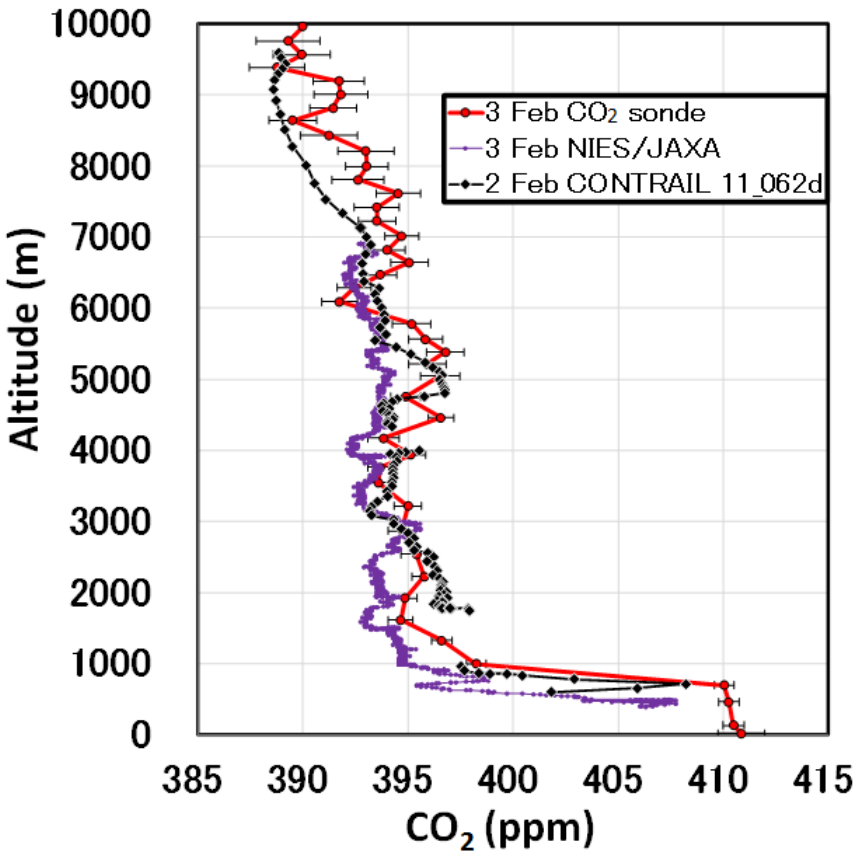

Figure 14. The CO_2 vertical profiles obtained by the CO_2 sonde (circles connected with red lines), NIES/JAXA chartered aircraft data (dots connected with purple lines) on 3 February, and CONTRAIL data (diamonds connected with black lines) on 2 February 2011.

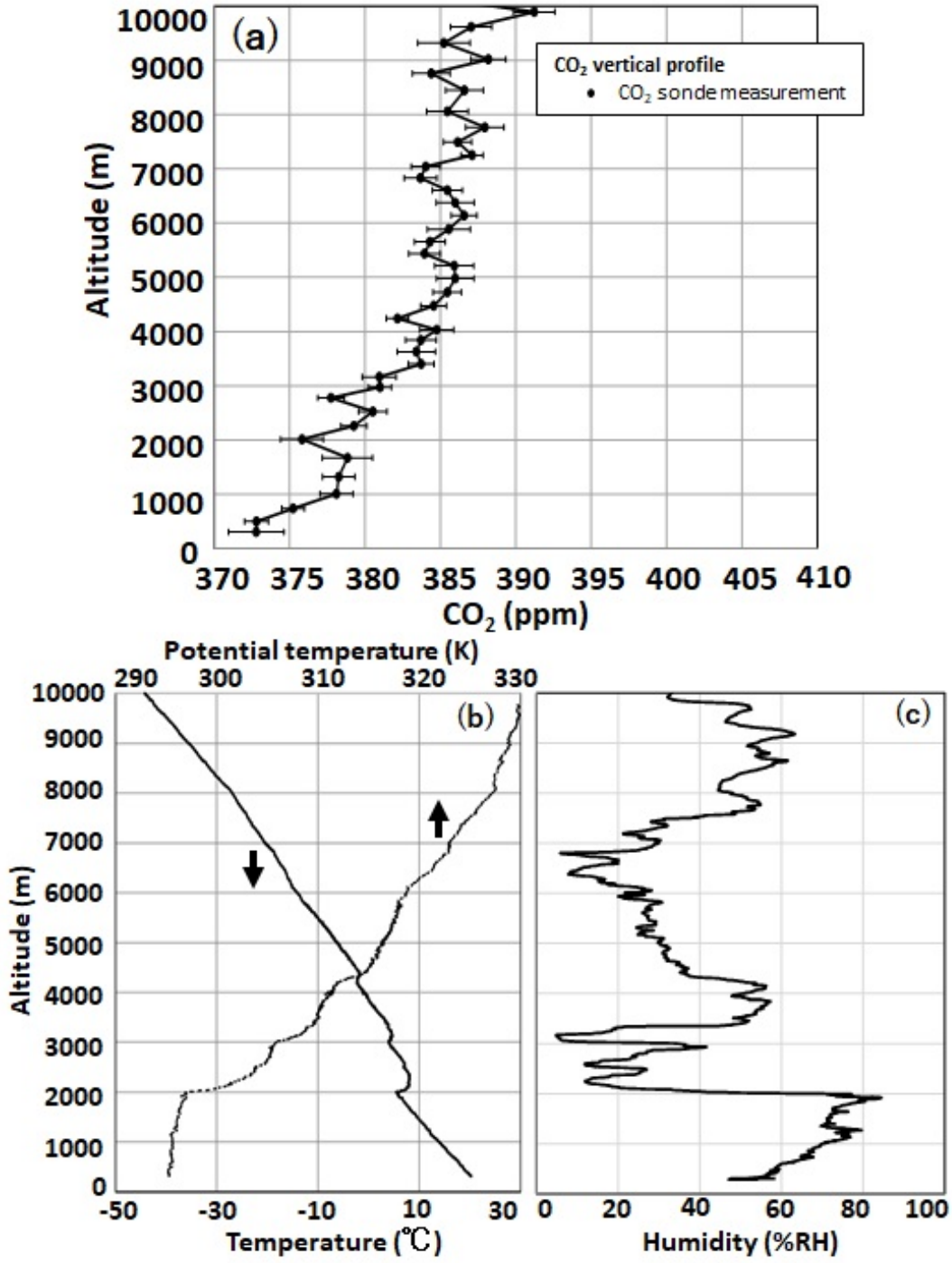

Figure 15. Profiles of (a) CO_2 mixing ratio, (b) temperature (solid line) and potential temperature (dotted line), and (c) relative humidity observed over a forest area, Moshiri in Hokkaido, Japan by the balloon launched on 26 August 2009 at 13:30 (LST). The black circles with error bars in panel (a) represent the data obtained by the CO_2 sonde.

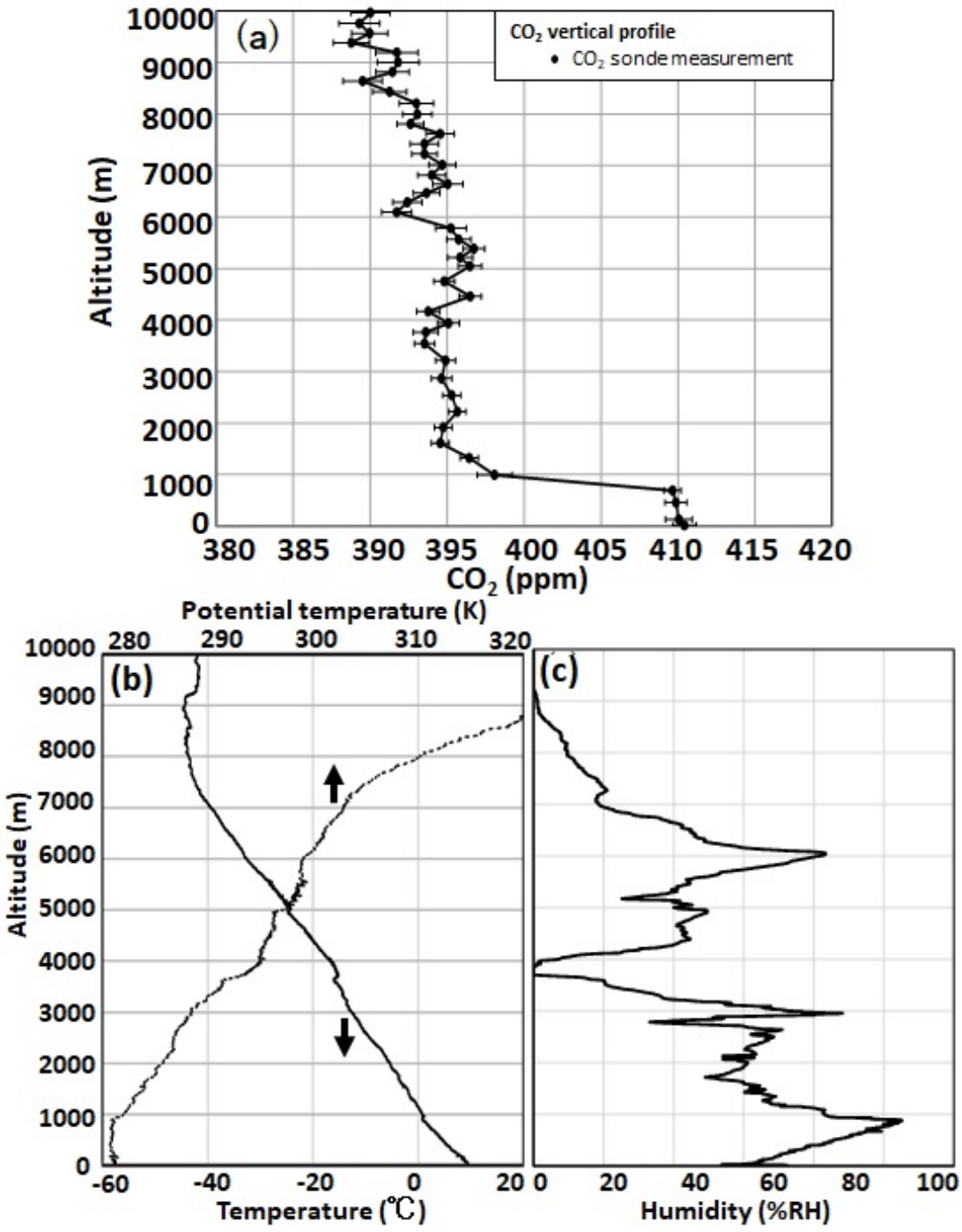

Figure 16. Profiles of (a) CO_2 mixing ratio, (b) temperature (solid line) and potential temperature (dotted line), and (c) relative humidity observed over an urban area, Moriya near Tokyo on 3 February 2011 at 13:10 (LST).

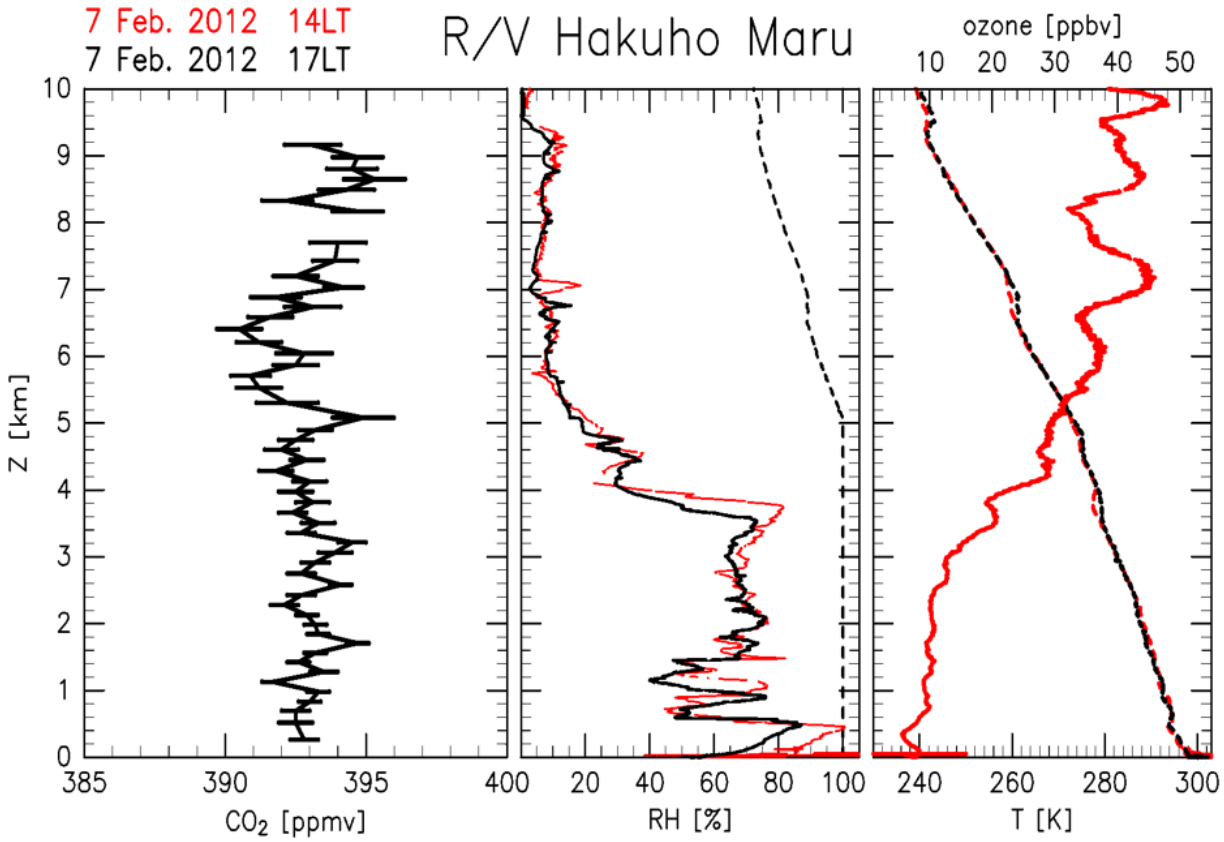

Figure 17. Vertical profiles of [left figure] CO_2, [center figure] relative humidity (RH) (solid lines) and ice-saturation RH (dashed line), and [right figure] ozone (red solid line) and temperature (black dashed line), taken on 07 February 2012, 00:14 (UT) from R/V Hakuho Maru in the equatorial eastern Pacific. Taken from Inai et al. (2018).

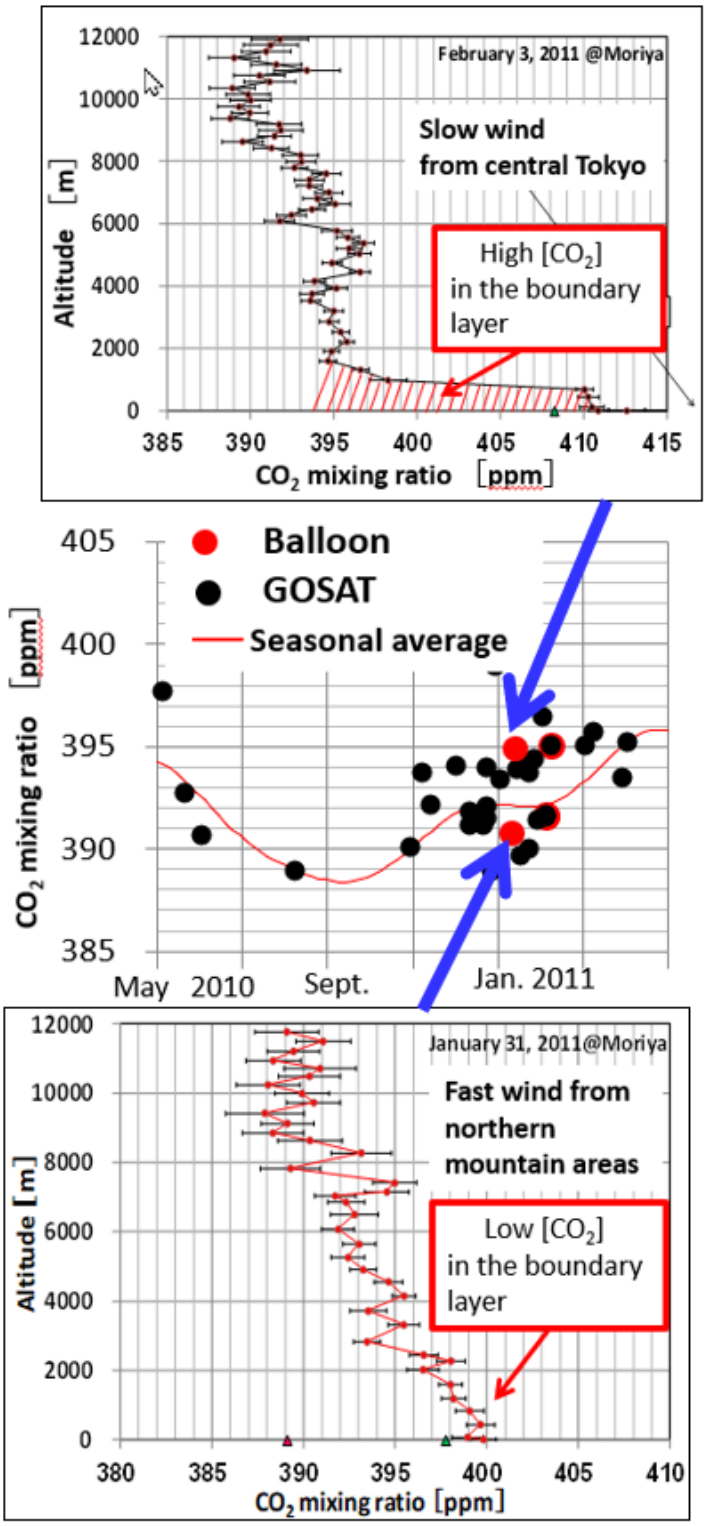

Figure 18. Vertical profiles on Feb. 3 (upper) and Jan. 31, 2011 (lower) obtained by the balloon-borne experiments and plots of column densities XCO_2 derived from the profiles and GOSAT satellite data.

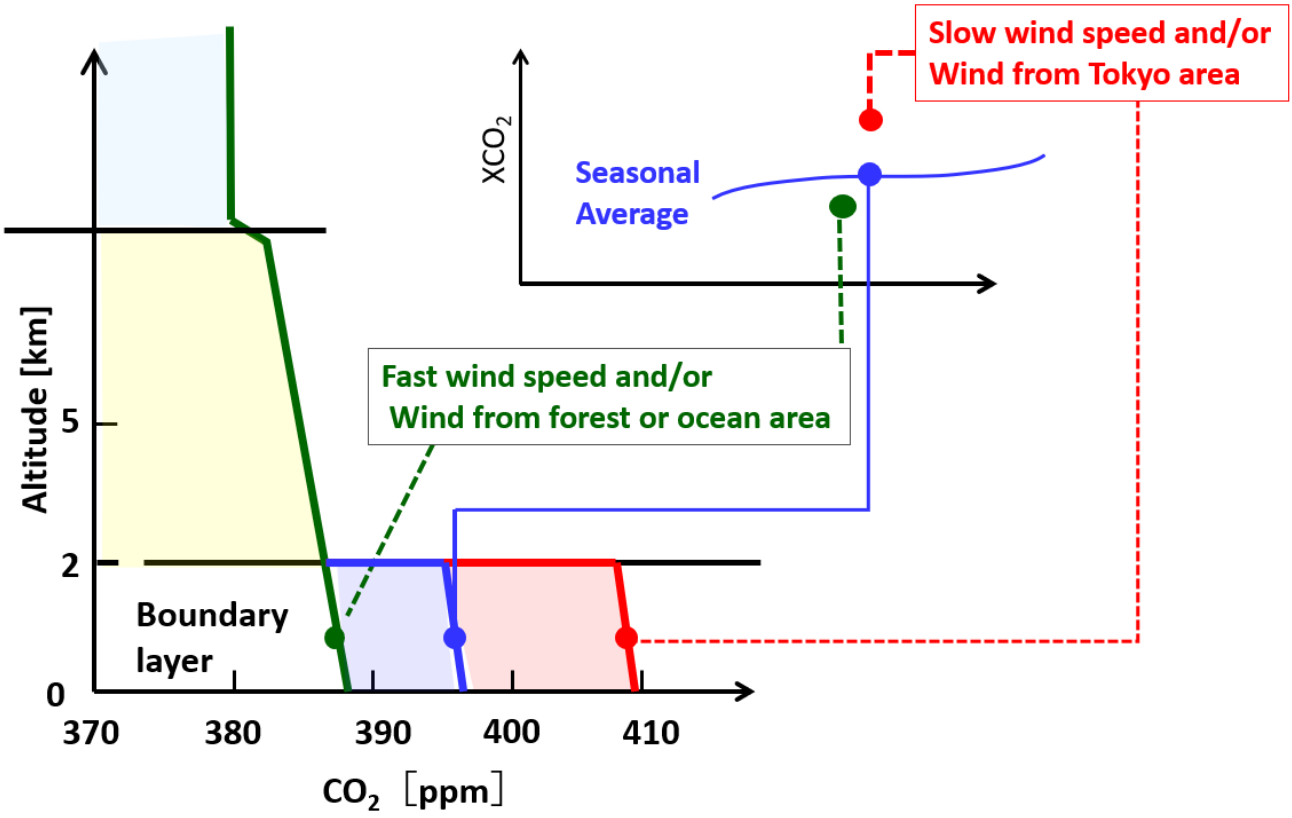

Figure 19. Schematic diagrams for the explanation of lower and higher XCO_2 values of GOSAT observation than the seasonal average curve, which are elucidated by the balloon-borne experiments.

Acknowledgements

The present work was conducted at the Institute for Space-Earth Environmental Research (ISEE) and Graduate School of Science, Nagoya University and I really appreciate the people who help me a lot for their cooperation and support in carrying out this study.

Foremost, I greatly appreciate the valuable comments from Prof. Matsumi Yutaka (Nagoya Univ.) and would like to thank him about technical assistance with the experiments. The authors would like to thank Prof. Matsumi for suggesting the topic treated in the paper and for providing substantial guidance. I am also very grateful to a lecturer Tomoki Nakayama (Nagoya Univ.) for most adequate advices and discussions, who helped me a lot with the experiments.

The author would like to thank Mr. N. Toriyama, M. Kanada, H. Jindo, M. Sera, H. Sasago, T. Ide, and S. Takekawa, and Drs. M. Kawasaki, G. Inoue (Nagoya Univ.), M. Fujiwara(Hokkaido Univ.), and Y. Inai (Tohoku Univ.), S. Aoki, and T. Nakazawa (Tohoku Univ.) for their sufficient assistance and meaningful suggestions in the development of CO_2 sonde and the observations. Without all the members of Matsumi laboratory support and unremitting help this thesis would not have been possible. Also, great advice and support from Dr. N. Saitoh, Dr. Y.Terao and Dr. Y. Kasai were important for me. They were greatly appreciated.

Finally, I would like to extend my indebtedness to my family for their endless love, understanding, support, encouragement and sacrifice throughout my study.